The oldest gnathostome teeth

Andreev, Plamen; Sansom, Ivan; Li, Qiang; Zhao, Wenjin; Wang, Jianhua; Wang, Chun-Chieh; Peng, Lijian; Jia, Liantao; Qiao, Tuo ; Zhu, Min

DOI:
10.1038/s41586-022-05166-2

The oldest gnathostome teeth

Plamen S. Andreev[1,2†], Ivan J. Sansom[3†], Qiang Li[1,2†], Wenjin Zhao[2,4,5], Jianhua Wang[1], Chun-Chieh Wang[6], Lijian Peng[1], Liantao Jia[2], Tuo Qiao[2,4], Min Zhu[2,4,5]*

[1]Research Center of Natural History and Culture, Qujing Normal University, Qujing 655011, Yunnan Province, China. [2]Key CAS Laboratory of Vertebrate Evolution and Human Origins, Institute of Vertebrate Paleontology and Paleoanthropology, Chinese Academy of Sciences (CAS), Beijing 100044, China. [3]School of Geography, Earth and Environmental Sciences, University of Birmingham, UK. [4]CAS Center for Excellence in Life and Paleoenvironment, Beijing 100044, China. [5]University of Chinese Academy of Sciences, Beijing 100049, China. [6]National Synchrotron Radiation Research Center, Hsinchu 30076, Taiwan.

*Corresponding author: zhumin@ivpp.ac.cn.

†These authors contributed equally to this work.

Summary paragraph

Mandibular teeth and dentitions are features of jawed vertebrates that were first acquired by the Palaeozoic ancestors[1-3] of living chondrichthyans and osteichthyans. The fossil record currently points to the latter part of the Silurian[4-7] (circa 425 million years ago) as a minimum date for the appearance of gnathostome teeth and to the evolution of growth and replacement mechanisms of mandibular dentitions in the subsequent Devonian Period[2,8-10]. Here we provide the earliest direct evidence for jawed vertebrates by describing *Qianodus duplicis*, a new genus and species of a lower Silurian gnathostome based on isolated tooth whorls from Guizhou Province, China. The whorls possess non-shedding teeth arranged in a pair of rows that demonstrate a number of features found in modern gnathostome groups. These include lingual addition of teeth in offset rows and maintenance of this patterning throughout whorl development. Our data extend the record of toothed gnathostomes by 14 million years from the upper Silurian into the lower Silurian (circa 439 million years ago) and are significant in documenting the initial diversification of vertebrates. They add to mounting fossil evidence supporting an earlier emergence of jawed vertebrates as part of the Great Ordovician Biodiversification Event.

Jawed fishes have a patchy and controversial fossil record through the Ordovician and the SIlurian[11,12]. The unequivocal evidence for their first appearance is currently constrained by the discovery of upper Silurian (c. 428–420 million years ago) 'placoderms'[13-15] and stem sarcopterygians[7,11] from South China and Vietnam and the disarticulated remains of the stem osteichthyans *Andreolepis* and *Lophosteus* from Europe and North America[4,5]. The earliest remains of chondrichthyans (elasmobranchs, holocephalans and their 'acanthodian' ancestors) include body fossils from the upper Silurian[16] and Lower Devonian[17-20], isolated teeth of upper Silurian[21,22] and basal Devonian[23] age and, more contentiously[11,24], isolated scales and fin spines from the Ordovician[12] and Silurian[25,26]. Convergence of scale-based characters and the paucity of available data[12,27] have further hampered the assignment of these fragmentary specimens to jawed vertebrates. Their incorporation into phylogenetic analyses has underscored this ambiguity by producing tree topologies[12] that are incongruent with the composition of the chondrichthyan stem and crown groups established from articulated fossils[24,28].

The present study describes tooth whorls from the Llandovery (Aeronian), lower Silurian of China (Fig. 1) that provide much-needed data on the dental conditions of early toothed vertebrates. With the investigation of the whorls we seek to 1) characterise their tooth patterning and morphological features, 2) provide a phylogenetic hypothesis for their affinities, and 3) highlight their implications for the timing of the origin and the diversification of jawed vertebrates during the Palaeozoic.

Systematic palaeontology

Gnathostomata Gegenbaur, 1874 (ref.[29])

Chondrichthyes Huxley, 1880 (ref.[30]) sensu Coates et al.[24]

Qianodus duplicis gen. et sp. nov.

Etymology: The generic name is a composite of *Qian*, referring to the ancient Chinese name of present-day Guizhou Province, and the Greek *odus*, meaning tooth. The specific name *duplicis* (double) alludes to the paired tooth rows of the whorls and derives from the genitive case of the Latin ‘duplex’.

Holotype: Isolated tooth whorl IVPP V26641 (Figs. 1c–f and 2a, f and Extended Data Fig. 2b, c, e).

Referred material: Twenty-three tooth whorls (including the holotype).

Locality and horizon: Section through the Rongxi Formation at Leijiatun village (Shiqian County), Guizhou Province, China (Fig. 1a, b). *Ozarkodina guizhouensis* conodont biozone (c. 439 Ma; late Aeronian, Llandovery, Silurian; see supplementary information).

Diagnosis: A jawed vertebrate possessing tooth whorls with primary teeth organized into two mutually offset rows. Lateral sides of the whorl base carry accessory tooth rows positioned lower than the primary teeth.

Remarks: The recovered *Qianodus* specimens co-occur in the Rongxi Formation together with disarticulated scales and fin spines of other yet-to-be-described acanthodian-grade[28] taxa. The available evidence does not allow us to categorically confirm or rule out attribution of any of this material to *Qianodus* given the preservation of the whorls as isolated elements and the development of tooth whorls in a number of 'acanthodian' lineages[31]. Our decision to erect a new taxon for the tooth whorls follows established practice[9] of formally describing isolated dental elements of Palaeozoic chondrichthyans if they are identifiable by a unique set of features.

Tooth whorl morphology and tissue structure

Specimens referred to *Qianodus duplicus* gen. et sp. nov. are up to c. 2.5 mm long (Extended Data Fig. 3) and possess a pair of primary tooth rows borne on a raised medial crest of the whorl base (Figs. 1c, f, 2a, b, e and Extended Data Fig. 1g). Primary teeth have a staggered arrangement (Fig. 2a–c, e, f) and their size increases within the rows in a manner recorded in whorls with non-shedding teeth where consistently larger elements are added lingually[31,32]. Due to the offsetting, it can be determined that the more labial (progenitor) row is initiated before the adjacent (trailing) row (Fig. 2a, b), with the distinction between the two only possible in specimens preserving the diminutive early tooth generations. The whorls exhibit left and right configurations produced by 'mirror image' arrangements of the primary tooth rows (Fig. 2a, b). We interpret the progenitor row of either type as occupying a mesial position based on comparison with modern elasmobranch dentitions[33,34] that possess alternate patterning of transverse tooth rows.

Most undamaged whorl bases have a deep, dome-like appearance, although the two smallest specimens exhibit recurved, low profiles (Extended Data Fig. 1j–n). The lateral faces of whorl bases carry rows of accessory teeth (Figs. 1, 2a–c, e, 3c and Extended Data Fig. 1j, k) distributed on arched ridges that follow the curvature of the whorl crest. The earliest formed generations of accessory teeth within each row are positioned at the inturned tip of the whorl spiral labially of the primary teeth (Fig. 2c, e and Extended Data Fig. 1a, d, j, k). Unlike the offset primary teeth, they are organised in closely set symmetrical pairs and are distinguished on that basis. The accessory tooth fields lack the alternate arrangement of primary teeth but demonstrate their characteristic labial increase in tooth size along individual rows. At corresponding positions accessory teeth are consistently smaller than the primary teeth of the whorl crest.

Due to dissolution and recrystallization, the microstructure of tooth whorl tissues is largely obscured by diagenetic artefacts. These preclude the identification of tissue types. Only large-calibre vascular spaces are apparent inside the whorls.

Whorl teeth demonstrate pulp-like spaces infilled by radiopaque crystalline (Fig. 2d) and radiotransparent globular (Extended Data Fig. 2g, h) material. These fabrics also account for the extensive recrystallisation of the tooth walls where they exploit voids created by diagenetic dissolution of the mineralised tissue (Fig. 2d).

Tooth whorl bases are composites of a superficial spongiose tissue and an inner compact tissue (Fig. 2d, f and Extended Data Fig. 2). The spongiosa is best developed along the medial crest of the whorl and diminishes in thickness down its sides and lingually (Fig. 2d, f and Extended Data Fig. 2a, b, d). Along the whorl crest it forms socket-like depressions housing the ankylosed to the base attachment portion of primary teeth (Fig. 2d, f and Extended Data Fig. 2a–d). Volume renderings of the spongiosa reveal an extensive system of canal-like spaces that follow the curvature of the whorl (Fig. 2d, f and Extended Data Fig. 2c). The canals are intercepted by the pulps of the whorl teeth and connect successive tooth generations of the primary and accessory rows (Fig. 2f and Extended Data Fig. 2c, f).

The compact zone of the base is thickest labially and tapers off lingually. The superimposed spongiosa extends over the compact zone on all sides to form the base periphery (Fig. 2d, f and Extended Data Fig. 2a, b, d, e). No histological data could be retrieved from the compact tissue, as its original structure is replaced by globular diagenetic material (Fig. 2d and Extended Data Fig. 2a).

Growth of the tooth whorls

Two of the whorls (Extended Data Fig. 1j–n) are recognised as early developmental stages, as these are of markedly smaller size, have fewer tooth rows/generations and shallower base profiles than the rest of the recovered specimens (Extended Data Fig. 3). This interpretation is further supported by the correspondence between the spacing and size of their teeth and those carried by the labial end of the whorl spiral of the larger ontogenetically older specimens. The early development whorls possess only the first, orally facing, pair of accessory rows, which contain one less tooth per row in comparison to their primary tooth rows (2 versus 3). Mature whorls (Fig. 2c) similarly have the largest number of tooth generations (maximum of 8) present within the primary rows and exhibit progressively decreasing tooth counts in the first, second and lower accessory rows (Fig. 2e). These observations suggest that the first formed whorl teeth were those of the primary tooth rows, with the inception of accessory rows occurring later in development in a sequence following the expansion of the whorl base.

Qianodus in the context of vertebrate dentitions

Although the whorls of *Qianodus* show significant post-mortem abrasion and diagenetic alteration, the material allows direct comparison with the oropharyngeal teeth/denticles of gnathostomes. The pronounced curvature of the whorls and their ordered tooth rows contrast with the aggregates of pharyngeal denticles of the type developed by thelodont jawless stem-gnathostomes[1,35]. The thelodont pharyngeal denticles constitute `sheets` of fused scales[1] that, although exhibiting polarity, lack the strictly unidirectional sequence of addition of the whorl teeth of *Qianodus* and their arrangement into discrete rows. Compound buccopharyngeal denticles have also been recorded in Palaeozoic symmoriid chondrichthyans[36,37] but similarly lack the arched profiles of tooth whorls. However, the spiral shape and longitudinal tooth rows of *Qianodus* are consistent with an origin within the dental groove of the jaw as elements that transverse the jaw rami[32,33,38]. Similarly, identification of the whorls as extraoral elements akin to the cheek scales found in ischnacanthid 'acanthodians'[39] is considered implausible, as these do not exhibit the spiral-like morphology of the whorls.

Possession of mandibular teeth, and by extension jaws, places *Qianodus* firmly within jawed vertebrates. Its phylogenetic position is further constrained by our parsimony analysis (Extended Data Figs. 4, 5) that recovers *Qianodus* as a derived stem chondrichthyan, in accord with a previously proposed origin of tooth whorls within crown gnathostomes[24,31,40].

Jawed stem gnathostomes, traditionally referred to as 'placoderms'[11], reveal that primitive vertebrate dentitions lacked discrete dental elements such as tooth whorls, but instead were composed of a few large toothed plates borne on the mandibular arches[3,8,15]. In one of their major divisions, the arthrodires, oral teeth develop radially or bidirectionally along the length of gnathal bones[10,41]. However, a recent investigation[3] of acanthothoracid 'placoderms' has identified lingual addition of replacement teeth directed within rows in the gnathal plates of *Kosoraspis*. The latter's labio-lingual tooth patterning is comparable to that of tooth whorls but, similarly to the dentition of some arthrodires[41,42], *Kosoraspis* gnathal plates carry multiple tooth rows whose number is not constantly maintained across all plates.

The disarticulated state of the material and its poor histological preservation allows *Qianodus* to be coded only for a limited set of dental characters (Supplementary Data 6). Improving the robustness of the phylogenetic hypothesis (Extended Data Figs. 4, 5) will depend on new information on the detailed histology of the whorls of *Qianodus*, as well as the currently missing data on the morphology of the fish. These could potentially be collected by further sampling of the Rongxi Formation and coeval assemblages[14].

Data from whorl-forming chondrichthyans and osteichthyans (Fig. 3) places the dentition of *Qianodus* within a broader phylogenetic context. Within osteichthyans, tooth whorls are documented mostly among the stem sarcopterygians where they are restricted to parasymphyseal positions[38,43,44] of the inner dental arcade[44]. Sarcopterygian whorls carry a medial row of similar-sized teeth that are shed repeatedly at the labial end of the whorl[38,43]. Recurring tooth replacement through hard-tissue resorption also occurs in the tooth cushions of the stem osteichthyans *Andreolepis* and *Lophosteus*[4,5]. These are, akin to tooth whorls, elements of the inner dental arcade with a non-mineralised attachment to the jaw ramus[5]. Tooth cushions support multiple tooth rows within which replacement teeth are deposited on top of resorbed older tooth generations[4,5]. The resorptive tooth shedding of osteichthyan parasymphyseal whorls and tooth cushions[4,5,43], nevertheless, contrasts with the tooth retention seen in the whorls of *Qianodus* (Figs. 1, 2). Tooth retention is seen in the tooth whorls of chondrichthyans[31] and it is most parsimonious to look among these for a 'template' of the dentition of *Qianodus*.

In the chondrichthyan total group tooth whorls are restricted to symphyseal and/or parasymphyseal positions[9,19] or can also be found along the lateral extent of the jaw as the only elements of the dentition[18,32,45,46] (Fig. 3). The asymmetry of tooth offsetting and its mirroring in *Qianodus* whorls (Fig. 2a, b) points to their origin from lateral positions on both jaw rami rather than formation on the jaw symphysis. An alternative explanation for *Qianodus* whorls as symphyseal and/or parasymphyseal elements is considered less credible as single tooth rows occupy each of these positions in crown gnathostomes with whorls confined to the jaw symphysis[19,38]. Moreover, the size differences between *Qianodus* whorls of comparable stage of development are consistent with the mesial enlargement of whorl dimensions along the jaw ramus observed in the stem chondrichthyan *Doliodus*[32] (Extended Data Fig. 3). Whorl-based dentitions occur in the climatiids (e.g. *Ptomacanthus* and *Climatius*[17,18]) and in *Doliodus*[32] (Fig. 3) and represent the stem chondrichthyan condition for developing tooth rows that traverse the jaw rami (Fig. 3). Tooth retention in whorls is also documented in the chondrichthyan crown group within holocephalans[47] (Extended Data Fig. 4), notably in lateral positions as inferred for *Qianodus*. The latter's possession of compound whorls is indicative of the competence of tooth rows to fuse into complex units and exhibit alternate patterning during ontogeny at lateral positions of the dentition. It remains to be determined whether similar offsetting occurs between adjacent single-tooth-row whorls in climatiids (e.g. *Ptomacanthus*[17]) and, potentially, in other more crown-ward[24] stem chondrichthyans (*Doliodus*[32]).

The presence of tooth whorls in the lower Silurian extends the minimum age for the origin of vertebrate jaws and dentitions back by approximately 13 million years (Extended Data Fig. 4) to close to the Ordovician–Silurian boundary. In addition, *Qianodus* partially infills and explains a gap in the fossil record between putative gnathostome scales and fin spines from the Upper Ordovician–lower Silurian[11,12,26,48] and the appearance of teeth in the upper Silurian[6,7,21,22]. The paucity of teeth and dental elements recorded through this interval may result from their extremely low abundance (as evident from the Rongxi Formation collections – see Methods), coupled with the challenges in differentiating between isolated oral and extraoral elements of unconventional morphologies[3,5,24,39]. *Qianodus* presents rare, and some of the clearest to date, evidence supporting a proposed[11,12] appearance of jawed vertebrates during the Great Ordovician Biodiversification Event (c. 485 to 443 Ma[49]). Our phylogenetic analysis places *Qianodus* in the chondrichthyan total group, with the implication that a range of jawed fishes appeared in the Upper Ordovician and lower Silurian and co-existed alongside jawless vertebrates shortly after the inception of biomineralization in the gnathostome total group.

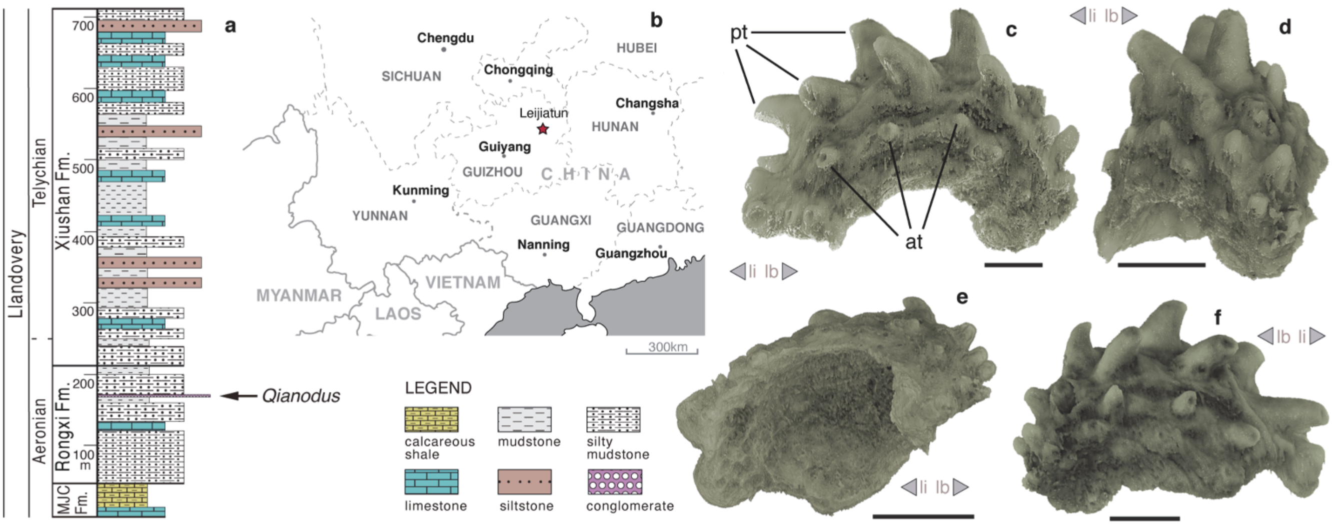

Fig. 1 | ***Qianodus duplicis* tooth whorls and their position in the Rongxi Formation exposed at Leijiatun (Shiqian-Tunping section), Guizhou Province, China.** (**a**) Chronostratigraphy and lithostratigraphy of the Shiqian-Tunping section and (**b**) a map showing its location. (**c** to **f**) Volume renderings of synchrotron X-ray tomography data depicting the holotype of *Qianodus* IVPP V26641 in (**c**) distal, (**d**) labial, (**e**) basal and (**f**) mesial lingual views. at, accessory teeth; la, labial; li, lingual; pt, primary teeth. Scale bars, 0.5 mm.

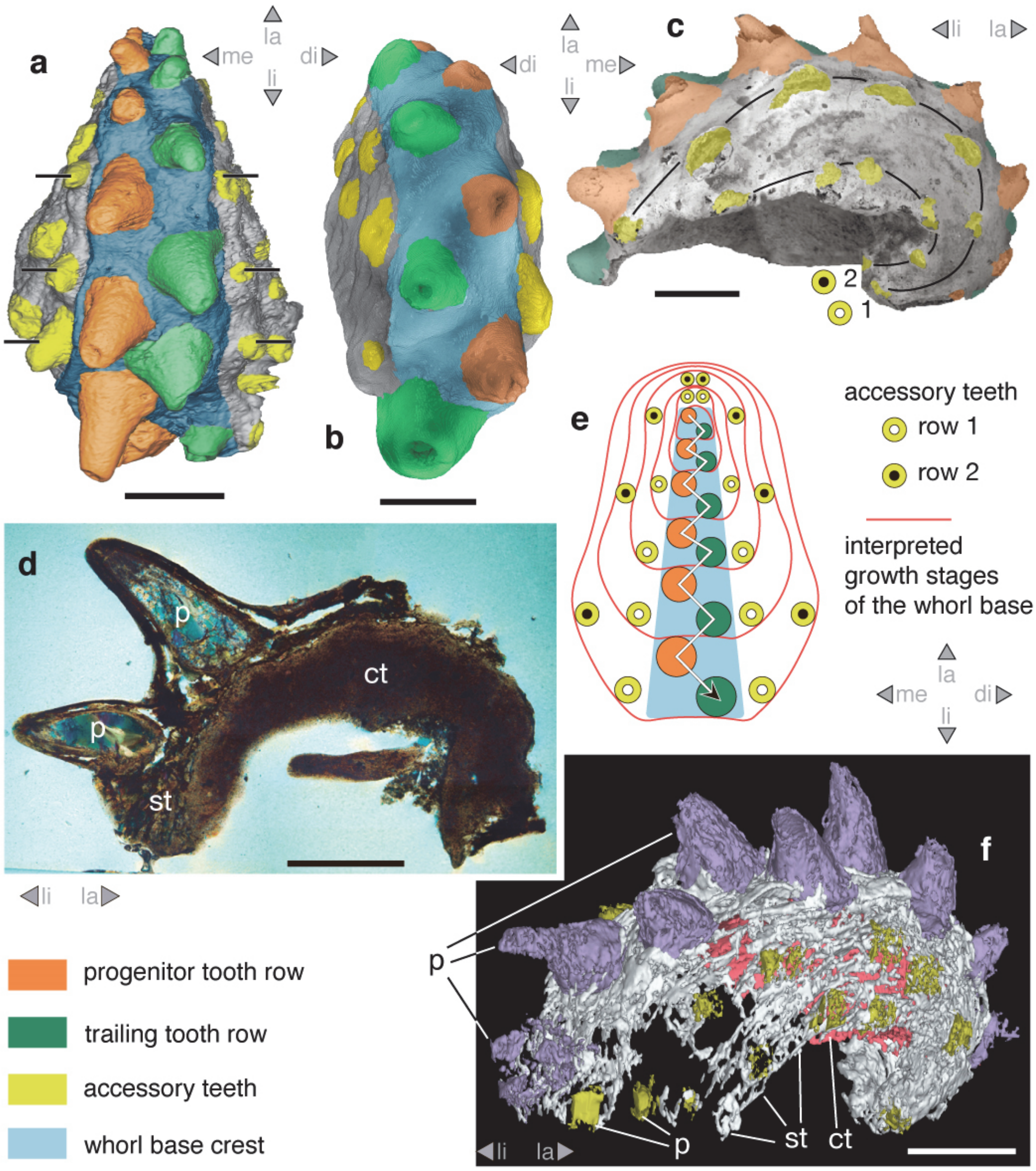

Fig. 2 | Tooth patterning and tissue structure of *Qianodus duplicis* whorls. Volume renderings of X-ray (**a**, **f**) synchrotron and (**b**) microcomputed tomography data**,** (**c**) scanning electron microscopy and (**d**) Nomarski DIC optics microscopy. Oral views of whorls with (**a**) left (holotype IVPP V26641) and (**b**) right (IVPP V26647) progenitor tooth families. Black horizontal lines in (a) indicate the alignment between the accessory tooth rows located closest to the primary teeth. (**c**) Mesial view of a whorl specimen (IVPP V26649) preserving evidence for the position of all primary and accessory teeth (black lines trace the course of accessory tooth rows 1 and 2). (**d**) Longitudinal thin section of a tooth whorl IVPP V26644. (**e**) Summary diagram of tooth arrangement and growth pattern of *Qianodus* whorls. (**f**) Vascular system of the holotype IVPP V26641 shown in labial distal view (purple, primary teeth; yellow, accessory teeth). ct, compact tissue; di, distal; la, labial; li, lingual; m, mesial; p, tooth pulp; st, spongiose tissue. Scale bars, 0.5 mm.

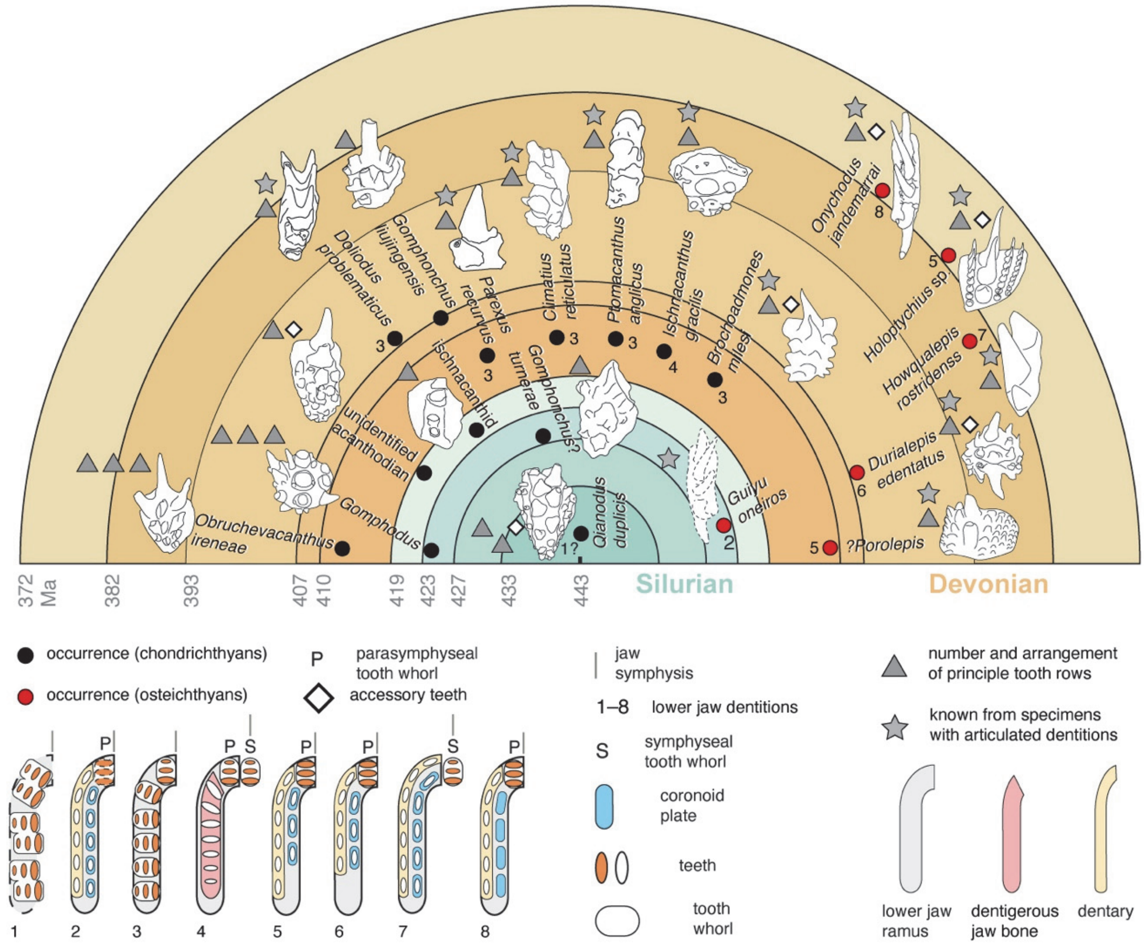

Fig. 3 | **Examples of the earliest chondrichthyan and osteichthyan tooth whorls.** The diagram illustrates oral views of tooth whorl morphologies from the Silurian–Middle Devonian and their position in lower jaw dentitions. Dashed-line margins of dentition symbols indicate unknown elements. Question mark next to *Qianodus* denotes indirect support for proposed dentition patterning. Presence of parasymphyseal whorls in *Guiyu* is indirectly supported by possession of jaw articulations surfaces for parasymphyseal plates[7]. See Supplementary information for details about the line art and data presented in the figure.

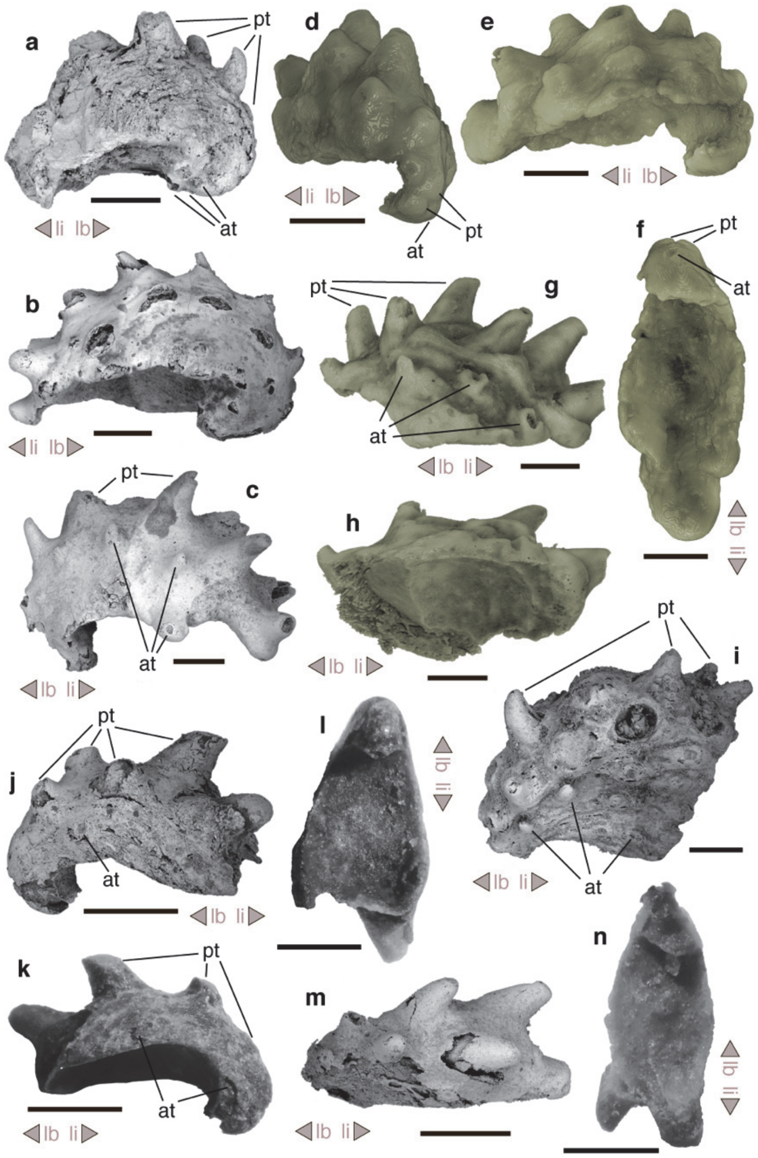

Extended Data Fig. 1 | Morphology of *Qianodus* tooth whorls. (**a–c, i, j, m**) Scanning electron microscopy, volume renderings of (**g**, **h**) synchrotron and (**d–f**) microcomputed X-ray tomography datasets and (**k, l, n)** light microscopy. (**a**) Lateral (mesial or distal) view of a heavily abraded tooth whorl (IVPP V26648). (**b**) Mesial view of a tooth whorl (IVPP V26649). (**c**) Latero-posterior view of a tooth whorl (IVPP V26652). (**d–f**) Tooth whorl (IVPP V26647) in (d) labial, (e) mesial and (f) basal views. (**g**, **h**) Incomplete tooth (IVPP V26645) whorl in (g) mesial and (h) basal views. (i) Lateral view of a tooth whorl (IVPP V26654) with a flared-out base. (**j**–**n**) Two complete whorls with 6 recognizable primary teeth in (**j, k**) lateral (distal and mesial) (IVPP V26650), (**m**) oral (IVPP V26651) and (**l**, **n**) basal (IVPP V26650, 51) views. at, accessory teeth; la, labial, li, lingual; pt, primary teeth. Scale bars, 0.5 mm.

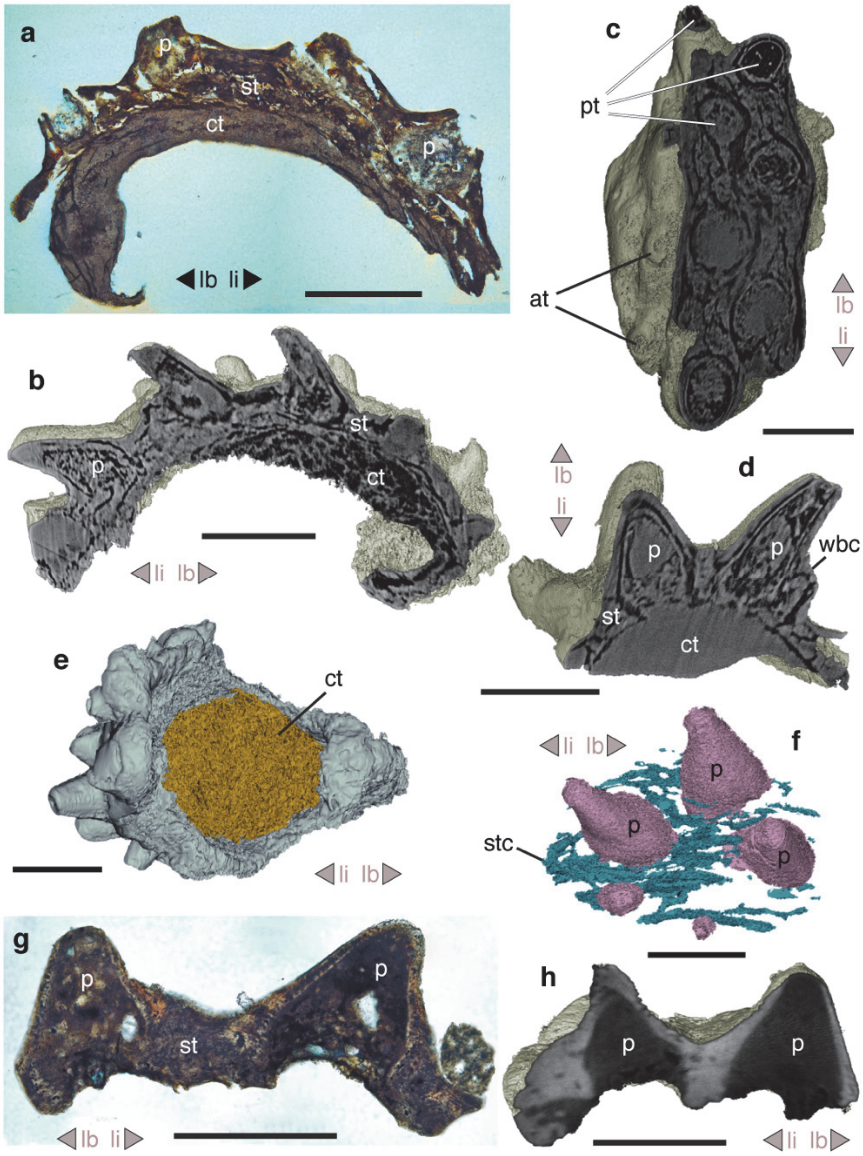

Extended Data Fig. 2 | Internal structure of *Qianodus* tooth whorls. (**a**, **g**) Nomarski DIC optical microscopy and (**b–f**, **h**) volume renderings of synchrotron X-ray tomography datasets. (**a**) Longitudinal thin section through a whorl with partially preserved teeth IVPP V26653. (**b**) Longitudinal virtual slice through the progenitor tooth row of the holotype IVPP V26641. (**c**) Horizontal virtual slice through the holotype IVPP V26641 at the level of tooth. (**d**) Transverse virtual slice through a partially preserved whorl IVPP V26645. (**e**) Basal view of IVPP V26641 with highlighted compact tissue of the base. (**f**) Volume rendering of radiotransparent structures inside a tooth whorl fragment (IVPP V26646) shown in oral view. (**g**) Longitudinal thin section and (**h**) longitudinal virtual section through IVPP V26646. at, accessory teeth; ct, compact tissue; la, labial; li, lingual; p, tooth pulp; pt, primary teeth; st, spongiose tissue; stc, spongiose tissue canals; wbc, whorl base crest. Scale bars, 0.5 mm.

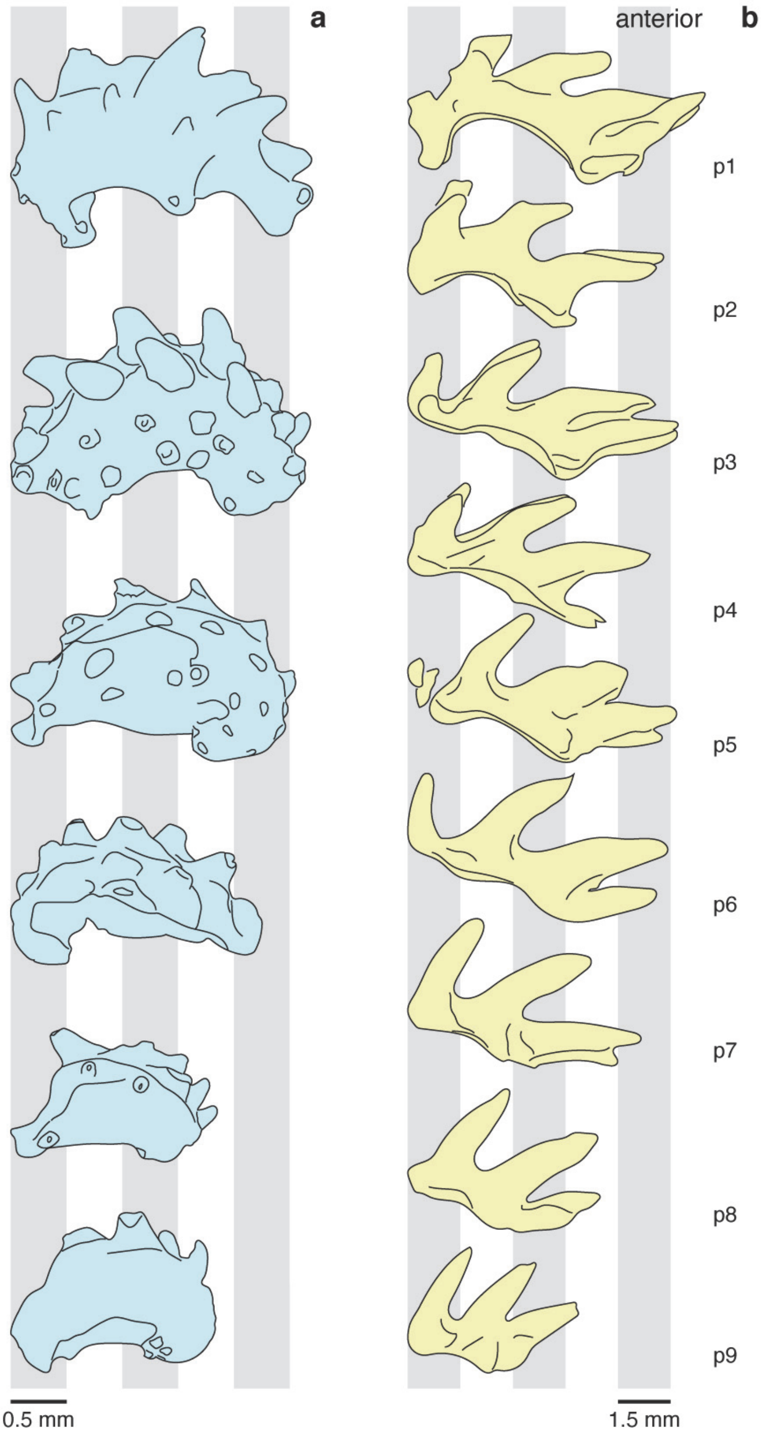

Extended Data Fig. 3 | Comparison of *Qianodus* tooth whorls with the whorl-based dentition of the stem chondrichthyan *Doliodus problematicus*. (a) *Qianodus* tooth whorls at a late stage of development (from top to bottom IVPP V26652, V26641, V26649, V26647, IV26655 and V26648). (**b**) Tooth whorls of the lower left jaw ramus of *Doliodus* at positions 1 to 9 (P1–9) (adapted from Maisey et al.[32]).

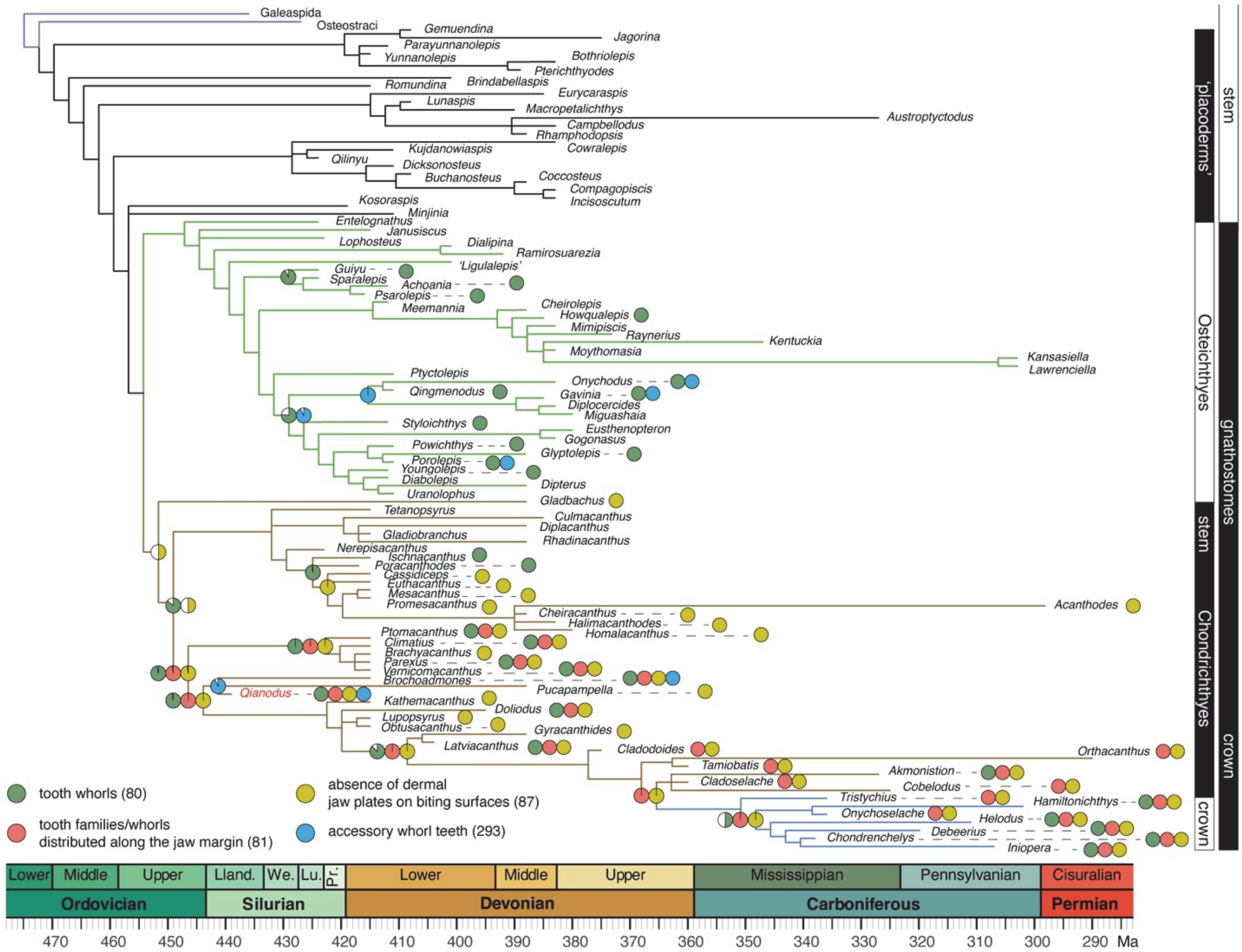

Extended Data Fig. 4 | Phylogenetic position of *Qianodus* within early jawed vertebrates. 50 percent majority-rule consensus tree from a parsimony analysis of 105 taxa and 294 characters. Tree time-adjusted using minimum branch length scaling. Taxon and tree root ages sourced from King et al.[50] and other studies (see Extended Data Table 1). Colour coding of cladogram branches: jawless stem gnathostomes (purple), 'placoderms' (black), Osteichthyes (green), stem Chondrichthyes (ochre), crown Chondrichthyes (blue). Pie charts represent Markov k-state 1 likelihood values for tooth whorl/dentition characters at select internal nodes. Circles show character states at terminal nodes. Character numbers shown in parentheses.

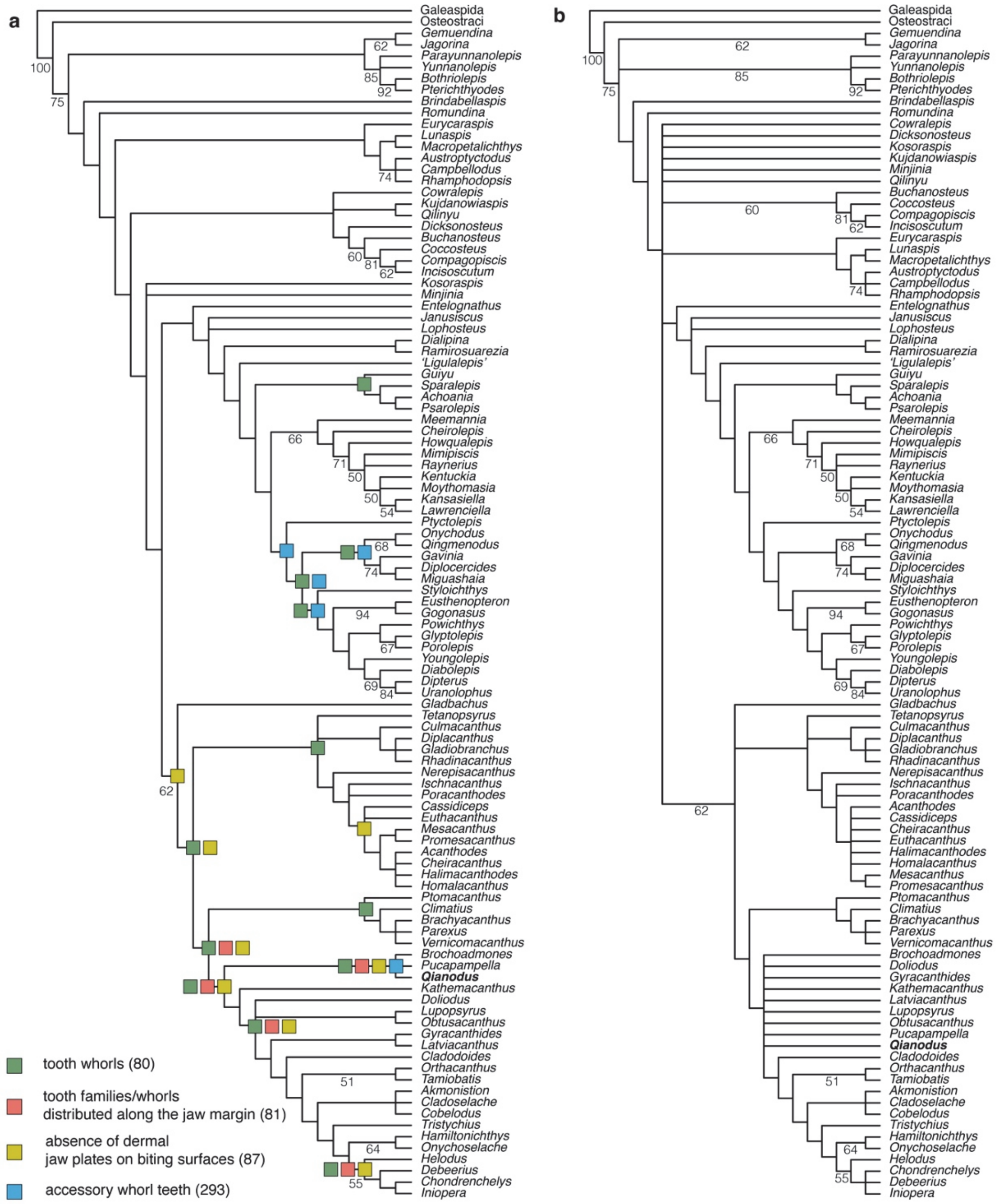

Extended Data Fig. 5 | Results of the parsimony analysis described in the Methods section and in Extended Data Fig. 4. (**a**) 50% majority-rule consensus and (**b**) strict consensus tree topologies. Squares in (**a**) depict most-parsimonious character state reconstructions at select internal nodes (character numbers shown in parentheses). Numbers at internal branches represent bootstrap values of 50 percent and above.

Online content

Any methods, additional references, Nature Research reporting summaries, source data, extended data, supplementary information, acknowledgements, peer review information; details of author contributions and competing interests; and statements of data and code availability are available at https://doi.org/XXXXX

1 Donoghue, P. C. & Rücklin, M. The ins and outs of the evolutionary origin of teeth. *Evol. Dev.* **18**, 19-30 (2016).

2 Smith, M. M. Vertebrate dentitions at the origin of jaws: when and how pattern evolved. *Evol. Dev.* **5**, 394-413 (2003).

3 Vaškaninová, V. *et al.* Marginal dentition and multiple dermal jawbones as the ancestral condition of jawed vertebrates. *Science* **369**, 211-216 (2020).

4 Chen, D., Blom, H., Sanchez, S., Tafforeau, P. & Ahlberg, P. E. The stem osteichthyan *Andreolepis* and the origin of tooth replacement. *Nature* **539**, 237-241 (2016).

5 Chen, D. *et al.* Development of cyclic shedding teeth from semi-shedding teeth: the inner dental arcade of the stem osteichthyan *Lophosteus*. *R. Soc. Open Sci.* **4**, 161084 (2017).

6 Choo, B., Zhu, M., Zhao, W. & Jia, L. The largest Silurian vertebrate and its palaeoecological implications. *Sci. Rep.* **4**, 5242 (2014).

7 Zhu, M. *et al.* The oldest articulated osteichthyan reveals mosaic gnathostome characters. *Nature* **458**, 469-474 (2009).

8 Denison, R. H. *Placodermi*. Vol. 2 (Gustav Fischer Verlag, 1978).

9 Ginter, M., Hampe, O., Duffin, C. J. & Schultze, H. *Handbook of Paleoichthyology Volume 3D. Chondrichthyes. Paleozoic Elasmobranchii: Teeth* (Verlag Dr Friedrich Pfeil, 2010).

10 Rücklin, M. *et al.* Development of teeth and jaws in the earliest jawed vertebrates. *Nature* **491**, 748-751 (2012).

11 Brazeau, M. D. & Friedman, M. The origin and early phylogenetic history of jawed vertebrates. *Nature* **520**, 490-497 (2015).

12 Sansom, I. J. & Andreev, P. S. in *Evolution and Development of Fishes* (eds Johanson, Z., Underwood, C. & Richter, M.) 59-70 (Cambridge Univ. Press, 2019).

13 Thanh, T.-D., Phuong, T. H., Boucot, A. J., Goujet, D. & Janvier, P. Silurian vertebrates from Central Vietnam. *C. R. Acad. Sci. Series IIA* **12**, 1023-1030 (1997).

14 Zhao, W.-J. *et al.* A review of Silurian fishes from north-western Hunan, China and related biostratigraphy. *Acta Geol. Pol.* **68** (2018).

15 Zhu, M. *et al.* A Silurian maxillate placoderm illuminates jaw evolution. *Science* **354**, 334-336 (2016).

16 Burrow, C. J. & Rudkin, D. Oldest near-complete acanthodian: the first vertebrate from the Silurian Bertie Formation Konservat-Lagerstätte, Ontario. *PLoS One* **9**, e104171 (2014).

17 Brazeau, M. D. A revision of the anatomy of the Early Devonian jawed vertebrate *Ptomacanthus anglicus* Miles. *Palaeontology* **55**, 355-367 (2012).

18 Burrow, C. J., Davidson, R. G., Den Blaauwen, J. L. & Newman, M. J. Revision of *Climatius reticulatus* Agassiz, 1844 (Acanthodii, Climatiidae), from the Lower Devonian of Scotland, based on new histological and morphological data. *J. Vertebr. Paleont.* **35**, e913421 (2015).

19 Burrow, C. J., Newman, M., Den Blaauwen, J., Jones, R. & Davidson, R. The Early Devonian ischnacanthiform acanthodian *Ischnacanthus gracilis* (Egerton, 1861) from the Midland Valley of Scotland. *Acta Geol. Pol.* **68**, 335–362 (2018).
20 Maisey, J. *et al.* in *Evolution and development of fishes* (eds Johanson, Z., Underwood, C. & Richter, M.) 87-109 (Cambridge Univ. Press, 2019).
21 Burrow, C. J. & Simpson, A. J. A new ischnacanthid acanthodian from the Late Silurian (Ludlow, ploeckensis Zone) Jack Formation, north Queensland. *Mem. Queensl. Mus.* **38**, 383-396 (1995).
22 Gross, W. Mundzähne und hautzähne der acanthodier und arthrodiren. *Palaeontogr. Abt. A*, 1-40 (1957).
23 Martínez-Pérez, C. *et al.* Vascular structure of the earliest shark teeth. *Acta Geol. Pol.* **68**, 335-362 (2018).
24 Coates, M. I. *et al.* An early chondrichthyan and the evolutionary assembly of a shark body plan. *Proc. R. Soc B* **285**, 20172418 (2018).
25 Andreev, P. S. *et al.* The systematics of the Mongolepidida (Chondrichthyes) and the Ordovician origins of the clade. *PeerJ* **4**, e1850 (2016).
26 Andreev, P. S. *et al.* Early Silurian chondrichthyans from the Tarim Basin (Xinjiang, China). *PLoS One* **15**, e0228589 (2020).
27 Keating, J. N., Marquart, C. L. & Donoghue, P. C. Histology of the heterostracan dermal skeleton: insight into the origin of the vertebrate mineralised skeleton. *J. Morph.* **276**, 657-680 (2015).
28 Dearden, R. P., Stockey, C. & Brazeau, M. D. The pharynx of the stem-chondrichthyan *Ptomacanthus* and the early evolution of the gnathostome gill skeleton. *Nat. Commun.* **10**, 1-7 (2019).
29 Gegenbaur, C. *Grundriss der vergleichenden Anatomie* (Wilhelm Engelmann, 1874).
30 Huxley, T. H. On the application of the laws of evolution to the arrangement of the Vertebrata, and more particularly of the Mammalia. *Proc. Sci. Meetings Zool. Soc. Lond.* **1880**, 649-662 (1880).
31 Rücklin, M. *et al.* Acanthodian dental development and the origin of gnathostome dentitions. *Nat. Ecol. Evol.* **5**, 919–926 (2021).
32 Maisey, J. G., Turner, S., Naylor, G. J. & Miller, R. F. Dental patterning in the earliest sharks: Implications for tooth evolution. *J. Morph.* **275**, 586-596 (2014).
33 Underwood, C., Johanson, Z. & Smith, M. M. Cutting blade dentitions in squaliform sharks form by modification of inherited alternate tooth ordering patterns. *R. Soc. Open Sci.* **3**, 160385 (2016).
34 Underwood, C. J. *et al.* Development and evolution of dentition pattern and tooth order in the skates and rays (Batoidea; Chondrichthyes). *PLoS One* **10**, e0122553 (2015).
35 Smith, M. M. & Coates, M. I. in *Major Events in Early Vertebrate Evolution* (ed Ahlberg, P. E.) 223-240 (Taylor & Francis, 2001).
36 Coates, M. & Sequeira, S. A new stethacanthid chondrichthyan from the Lower Carboniferous of Bearsden, Scotland. *J. Vertebr. Paleontol.* **21**, 438-459 (2001).
37 Zangerl, R. & Case, G. *Cobelodus aculeatus* (Cope), an anacanthous shark from Pennsylvanian black shales of North America. *Palaeontogr. Abt. A* **154**, 107-157 (1976).
38 Andrews, M., Long, J., Ahlberg, P., Barwick, R. & Campbell, K. The structure of the sarcopterygian *Onychodus jandemarrai* n. sp. from Gogo, Western Australia: with a functional interpretation of the skeleton. *Earth. Env. Sci. Trans. R. Soc. Edinb.* **96**, 197-307 (2005).
39 Blais, S. A., MacKenzie, L. A. & Wilson, M. V. Tooth-like scales in Early Devonian eugnathostomes and the ‘outside-in’ hypothesis for the origins of teeth in vertebrates. *J. Vertebr. Paleont.* **31**, 1189-1199 (2011).
40 Frey, L. *et al.* The early elasmobranch *Phoebodus*: phylogenetic relationships, ecomorphology and a new time-scale for shark evolution. *Proc. R. Soc. B* **286**, 20191336 (2019).

41 Hu, Y., Lu, J. & Young, G. C. New findings in a 400 million-year-old Devonian placoderm shed light on jaw structure and function in basal gnathostomes. *Sci. Rep.* **7**, 7813 (2017).
42 Hu, Y.-Z., Young, G., Burrow, C., Zhu, Y.-a. & Lu, J. High resolution XCT scanning reveals complex morphology of gnathal elements in an Early Devonian arthrodire. *Palaeoworld* **28**, 525-534 (2019).
43 Doeland, M., Couzens, A. M., Donoghue, P. C. & Rücklin, M. Tooth replacement in early sarcopterygians. *R. Soc. Open Sci.* **6**, 191173 (2019).
44 Zhu, M. & Yu, X. in: *Recent Advances in the Origin and Early Radiation of Vertebrates* (eds Arratia, G., Wilson, M. V. H. & Cloutier, R.) 271-286 (Verlag Dr. Friedrich Pfeil, 2004).
45 Burrow, C. J., Newman, M. J., Davidson, R. G. & den Blaauwen, J. L. Redescription of *Parexus recurvus*, an Early Devonian acanthodian from the Midland Valley of Scotland. *Alcheringa* **37**, 392-414 (2013).
46 Dearden, R. P. & Giles, S. Diverse stem-chondrichthyan oral structures and evidence for an independently acquired acanthodid dentition. *R. Soc. Open Sci.* **8**, 210822 (2021).
47 Zangerl, R. & Case, G. R. *Iniopterygia, a New Order of Chondrichthyan Fishes from the Pennsylvanian of North America* (Field Mus. Nat. Hist., 1973).
48 Andreev, P. S. *et al.* Upper Ordovician chondrichthyan-like scales from North America. *Palaeontology* **58**, 691-704 (2015).
49 Servais, T. & Harper, D. A. The great Ordovician biodiversification event (GOBE): definition, concept and duration. *Lethaia* **51**, 151-164 (2018).
50 King, B., Qiao, T., Lee, M. S., Zhu, M. & Long, J. A. Bayesian morphological clock methods resurrect placoderm monophyly and reveal rapid early evolution in jawed vertebrates. *Syst. Biol.* **66**, 499-516 (2017).

Methods

A total of 23 *Qianodus* tooth whorls of varying degrees of completeness were recovered from residues of Rongxi sample 35SQTP following disaggregation of c. 300 kg of sediment with buffered 8% acetic acid. The *Qianodus* specimens are among thousands of vertebrate microremains isolated from 35SQTP that await future investigation.

X-ray tomography

Synchrotron X-ray tomography analyses of three whorls (IVPP V26641 (Supplementary Data 3), V26645 (Supplementary Data 4), V26646)) were performed at BL01A1 and BL01B1 beamlines of the Taiwan Light Source (TLS), National

Synchrotron Radiation Research Center (NSRRC), Taiwan. Acquisition at ≥ 4 keV with a parallel semi-white-light hard X-ray beam over a 180° rotation arc generated datasets of 601 radiographs with pixel size of 2.76 μm. Post-acquisition, radiograph alignment was enhanced in Matlab R2014b by using the fast projection matching (Faproma) algorithm developed by Wang 2020[51]. Reconstructions of the radiograph data in VGSTUDIO MAX 3.0 produced sets of 1200 tomographic slices (1600 x 1600 pixels) per specimen.

One tooth whorl (IVPP V26647) was imaged at the Institute of Vertebrate Paleontology and Paleoanthropology, Chinese Academy of Sciences with an X-ray micro-computed tomography scanner (225-3D-μCT) designed by the Institute of High Energy Physics, Chinese Academy of Sciences [52]. The analysis produced 720 radiographs over a 360-degree rotation cycle that were converted in VGSTUDIO MAX 3.0 to a dataset of 1442 tomograms (each 1748 x 556 pixels at 5.33 μm per pixel). Three-dimensional visualization of the tomogram data from IVPP V26641 and IVPP V26645–V26647 was performed in Mimics 19.0 (Fig. 2a, f and Extended Data Fig. 2e, f, h), VGSTUDIO MAX 3.0 (Extended Data Fig. 2b–d) and in Drishti 2.6.5 (Fig. 1c–f and Extended Data Fig. 1d–h) from Mimics segmentation masks exported as DICOM files.

Scanning electron microscopy

Surface morphology of seven uncoated whorls (IVPP V26642, V26643, V26648–V26652) was documented with a Phenom ProX Desktop SEM at 5 keV at the School of Geography, Earth and Environmental Sciences, University of Birmingham.

Light microscopy

Doubly-polished sections of seven specimens (IVPP V26644, V26646, V26653–V26657) were investigated under DIC polarized light with an Olympus BX51 Fluorescence Microscope and documented with an Olympus D12 digital camera at Qujing Normal University, China.

Two tooth whorls (IVPP V26650, V26651) were imaged with a GXMXTL-3101 stereo microscope at the University of Birmingham, UK.

Phylogenetic analysis

TNT version 1.5[53] was used to perform a parsimony phylogenetic analysis based on a matrix of 294 characters and 105 taxa (Supplementary Data 6). The matrix was assembled from character data from Brazeau et al.[54], Coates et al.[24], Dearden[55], Dearden et al.[28], Dearden and Giles[46], Giles et al.[56], King et al.[50], Qiao et al.[57], Zhu et al.[15], Zhu et al.[58] and this study (character scores colour coded in the matrix nexus file, Supplementary Data 6). Characters were treated as unordered and of equal weights with Galeaspida being designated as an outgroup. Tree reconstruction was performed in TNT by a heuristic analysis using the mult search algorithm with tree-bisection-reconnection (TBR) branch swapping set to save 100 trees per replication and limited to 100 random addition-sequences. The search was set to retain 100000 trees and returned 100000 most parsimonious trees (940 steps each) from which 50% majority-rule consensus (944 steps) and strict consensus trees (1022 steps) were calculated (Supplementary Data 6).

Bootstrap support for internal tree nodes of the 50 percent majority-rule consensus and strict consensus trees was calculated in TNT via a traditional search method over 100 bootstrap replicates.

The 50 percent majority-rule consensus tree and its branch length values was imported into R (version 4.0.2) and time adjusted with the R package paleotree 3.3.25[59]. This analysis used the timePaleoPhy function of paleotree with mbl-type time scaling and pre-assigned taxon and tree root ages taken from King et al.[50] and other studies (Table 1).

Maximum likelihood scores for characters at internal nodes of the 50 percent majority-rule consensus tree were produced in Mesquite 3.51 (build 898) using a Markov k-state[11] probability model that assumes equal rates of character change.

Dentition data

Figure 3 dentition data and line art from this study and adapted from Andrews[38] (*Onychodus jandemarrai*), Botella et al.[60] (*Obruchevacanthus ireneae*), Burrow et al.[18] (*Climatius reticulatus*), Burrow et al.[45] (*Parexus recurvus*), Burrow et al.[19] (*Ischnacanthus gracilis*), Burrow and Simpson[21] (*Gomphonchus? turnerae*), Gagnier and Wilson[61] (*Brochoadmones milesi*), Gross[22] (*Gomphodus*), Jarvik[62] (*Holoptychius* sp.), Jarvik[62] (?*Porolepis*), Maisey et al.[32] (*Doliodus problematicus*), Long 1988[63] (*Howqualepis rostridens*), Miles[64] (*Ptomacanthus anglicus*), Mondéjar-Fernández et al.[65] (*Durialepis edentatus*), Qu et al.[66] (unidentified acanthodian), Vergoossen[67] (ischnacanthid), Wang[68] (*Gomphonchus liujingensis*) and Zhu et al.[7] (*Guiyu oneiros*).

Data availability

Supplementary files (Supplementary Data 1 to 6) are available at https://www.dropbox.com/sh/eor2wvwwbui25sk/AACckwBWZ9vyX5ouSdJ1aq27a?dl=0 and will be published online in a publicly accessible repository (Dryad) upon acceptance of the manuscript. Investigated *Qianodus* specimens were assigned accession numbers (IVPP V26641–V26663) and deposited at the Institute of Vertebrate Paleontology and Paleoanthropology (IVPP), Chinese Academy of Sciences, Beijing.

51 Wang, C.-C. Joint iterative fast projection Matching for fully Automatic Marker-free Alignment of nano-tomography Reconstructions. *Sci. Rep.* **10**, 7330 (2020).

52 Wang, Y. *et al.* Development and applications of paleontological computed tomography. *Vertebr. PalAsiat.* **57**, 84-92 (2019).

53 Goloboff, P. A. & Catalano, S. A. TNT version 1.5, including a full implementation of phylogenetic morphometrics. *Cladistics* **32**, 221-238 (2016).

54 Brazeau, M. *et al.* Endochondral bone in an Early Devonian 'placoderm' from Mongolia. *Nat. Ecol. Evol.*, **4**, 1477-1484 (2020).

55 Dearden, R. P. *The Anatomy and Evolution of "Acanthodian" Stem-chondrichthyans* (Imperial College London, 2018).

56 Giles, S., Friedman, M. & Brazeau, M. D. Osteichthyan-like cranial conditions in an Early Devonian stem gnathostome. *Nature* **520**, 82-85 (2015).

57 Qiao, T., King, B., Long, J. A., Ahlberg, P. E. & Zhu, M. Early gnathostome phylogeny revisited: multiple method consensus. *PLoS One* **11**, e0163157 (2016).

58 Zhu, Y.-a., Lu, J. & Zhu, M. Reappraisal of the Silurian placoderm Silurolepis and insights into the dermal neck joint evolution. *R. Soc. Open Sci.* **6**, 191181 (2019).

59 Bapst, D. W. paleotree: an R package for paleontological and phylogenetic analyses of evolution. *Methods Ecol. Evol.* **3**, 803-807 (2012).

60 Botella, H., Manzanares, E., Ferrón, H. & Martínez-Pérez, C. *Obruchevacanthus ireneae* gen. et sp. nov., a new ischnacanthiform (Acanthodii) from the Lower Devonian of Spain. *Paleontol. J.* **48**, 1067-1076 (2014).

61 Gagnier, P.-Y. & Wilson, M. V. An unusual acanthodian from northern Canada: revision of *Brochoadmones milesi*. *Mod. Geol.* **20**, 235-252 (1996).

62 Jarvik, E. Middle and Upper Devonian Porolepiformes from East Greenland with special reference to *Glyptolepis groenlandica* n. sp. and a discussion on the structure of the head in the Porolepiformes. *Medd. Grønl.* **187**, 1-307 (1972).

63 Long, J. New palaeoniscoid fishes from the Late Devonian and Early Carboniferous of Victoria. *Mem. Assoc. Australas. Palaeontol.* **7**, 1-64 (1988).

64 Miles, R. S. Articulated acanthodian fishes from the Old Red Sandstone of England: with a review of the structure and evolution of the acanthodian shoulder-girdle. *Bull. Br. Mu. Nat. Hist. Geol.* **24**, 111-213 (1973).

65 Mondéjar-Fernández, J., Friedman, M. & Giles, S. Redescription of the cranial skeleton of the Early Devonian (Emsian) sarcopterygian *Durialepis edentatus* Otto (Dipnomorpha, Porolepiformes). *Pap. Palaeontol.* (2020).

66 Qu, Q., Sanchez, S., Blom, H., Tafforeau, P. & Ahlberg, P. E. Scales and tooth whorls of ancient fishes challenge distinction between external and oral 'teeth'. *PLoS One* **8**, e71890 (2013).

67 Vergoossen, J. Late Silurian fish microfossils from Helvetesgraven, Skåne (southern Sweden)(I). *Geol. Mij.* **78**, 267-280 (1999).

68 Wang, N.-Z. Microremains of agnathans and fishes from Lower Devonian of central Guangxi with correlation of Lower Devonian between central Guangxi and eastern Yunnan, South China. *Acta Palaeontol. Sin.* **31**, 280-303 (1992).

Acknowledgements We thank Y.-M. Hou for the acquisition of the micro-CT X-ray data, Y. Hwu (Academia Sinica) and Y.-T. Weng (NSRRC) for performing and assisting with the synchtrotron X-ray analyses, and Y.Z. Hu for her comments and advice during the preparation of tooth whorl volume renderings in Drishti. This research was supported by the Strategic Priority Research Program of the Chinese Academy of Sciences (XDA19050102, XDB26000000), the National Natural Science Foundation of China (41530102), the Key Research Program of Frontier Sciences, CAS (QYZDJ-SSW-DQC002), an Open Project Grant of the Key Laboratory of Vertebrate Evolution and Human Origins, IVPP, CAS (LVEHO19001), MOST 108-2116-M-213-001 (Taiwan), Chinese Postdoctoral Science Foundation grant (2019M663440) and the National Synchrotron Radiation Research Center, Taiwan (beamtime Projects No 2019-3-083-1 and 2019-3-185-1).

Author contributions Research design: M.Z., P.S.A., and I.J.S.; Fieldwork and sample collection: M.Z., W.Z, Q.L., J.W., L.J., T.Q., and L.P.; Data processing: Q.L., P.S.A., L.P., J.W., and M.Z.; Synchrotron X-ray tomography analyses: P.S.A., and C.W.; Manuscript text and figure preparation: P.S.A., I.J.S., Q.L., J.W., and M.Z.

Competing interests The authors declare no competing interests.

Supplementary Information for:

The oldest gnathostome teeth

Plamen S. Andreev[1,2†], Ivan J. Sansom[3†], Qiang Li[1,2†], Wenjin Zhao[2,4,5], Jianhua Wang[1], Chun-Chieh Wang[6], Lijian Peng[1], Liantao Jia[2], Tuo Qiao[2,4], Min Zhu[2,4,5]*

[1]Research Center of Natural History and Culture, Qujing Normal University, Qujing 655011, Yunnan Province, China. [2]Key CAS Laboratory of Vertebrate Evolution and Human Origins, Institute of Vertebrate Paleontology and Paleoanthropology, Chinese Academy of Sciences (CAS), Beijing 100044, China. [3]School of Geography, Earth and Environmental Sciences, University of Birmingham, UK. [4]CAS Center for Excellence in Life and Paleoenvironment, Beijing 100044, China. [5]University of Chinese Academy of Sciences, Beijing 100049, China. [6]National Synchrotron Radiation Research Center, Hsinchu 30076, Taiwan.

*Corresponding author: zhumin@ivpp.ac.cn.

†These authors contributed equally to this work.

Geological setting and biostratigraphy of the Rongxi

The Rongxi Formation forms part of the laterally extensive and loosely defined 'lower marine red beds' that form a distinctive unit in South China. The Shiqian-Tunping (SQTP) section through the Rongxi is located N of Leijiatun village in Shiqian County, Guizhou Province (Fig. 1b). Here the unit is 242 m thick and consists of purple-red and grey mudstones interbedded with sporadic sandstone and carbonate units. Sample 35SQTP was collected from a c. 90 cm sequence of massive conglomerates alternating with mudstones within the upper half of the Rongxi Formation (Fig. 1a). The 35SQTP limestone conglomerate consists of well-rounded mudstone clasts (up to pebble size, c. 2 cm) and shell fragments/vertebrate remains bound by calcite cement. Previous paleoenvironmental interpretations of the Rongxi have concluded that it represents a shallow water intertidal depositional tract, referable to Benthic Assemblage Zone 1[1-3], and in this context the conglomerate dominated lens is readily recognized as a tidal channel deposit.

Age diagnostic fossils from the Rongxi outcrop at Leijiatun have largely been lacking, with invertebrate fossils being notably rare[4] and the age of the formation at Leijiatun and elsewhere has primarily been based upon the biostratigraphy of the underlying and overlying units. In part, this has led to the Rongxi being assigned to the late Aeronian[5-7], straddling the Aeronian-Telychian boundary, or the lower Telychian[3,8,9].

Sample 35SQTP has yielded the first conodonts to be recovered from the Rongxi and include platform elements of *Ozarkodina guizhouensis*[10], an index taxon for the *Ozarkodina guizhouensis* Biozone that covers the Aeronian–Telychian stage boundary. However, Wang et al.[7] and Wang[5] considered the conodont and graptolite evidence from the overlying Xiushan Formation to place the Rongxi in the Aeronian within the *Ozarkodina parahassi* division of the *O. guizhouensis* Biozone. We also regard it highly probable that the Lower Red Beds are diachronous throughout their 1000 kms of expression, with the outcrops in Guizhou, Hunan and Chongqing being older than the basal Telychian Formations in Sichuan and Shaanxi[3,8]. Thus, an Aeronian age for the Rongxi Formation at Leijiatun seems the most likely.

Character list for the phylogenetic analysis

Abbreviations of character sources: [B] Brazeau et al.[11], [C] Coates et al.[12], [D] Dearden et al.[13], [G] Giles et al.[14] and [K] King et al.[15].

1. [B:1] **Tessellate prismatic calcified cartilage.**
0 absent
1 present

2. [B:2] **Prismatic calcified cartilage.**
0 single layered
1 multi-layered

3. [B:3] **Perichondral bone.**
0 present
1 absent

4. [B:4] **Extensive endochondral ossification.**
0 absent
1 present

5. [B:5] **Enamel(oid) present on dermal bones and scales.**

0 absent
1 present

6. [B:6] **Enamel.**
0 single-layered
1 multi-layered

7. [B:7] **Enamel layers.**
0 applied directly to one another (ganoine)
1 separated by layers of dentine

8. [B:8] **Pore canal network.**
0 absent
1 present

9. [B:9] **Dentinous tissue.**
0 absent
1 present

10. [B:10] **Dentine kind (modified).**
0 mesodentine
1 semidentine
2 orthodentine

11. [B:11] **Bone cell lacunae in trunk scale bases.**
0 present
1 absent

12. [B:12] **Main dentinous tissue forming fin spine.**
0 osteodentine

1 orthodentine

13. [B:13] **Longitudinal scale alignment in fin webs.**

0 absent

1 present

14. [B:14] **Differentiated lepidotrichia.**

0 absent

1 present

15. [B:15] **Composition of trunk scale crowns (modified).**

Character 15 of Brazeau et al.[11] was reformulated to describe mono- and poly-odontode scale crowns on the basis of odontode number without alluding to their patterning.

0 comprising single odontode unit/generation ("monodontode")

1 comprising a complex of multiple odontode generations/units ("polyodontode")

16. [B:16] **Concentric addition of trunk scale odontodes (modified).**

Modified character 16 of Brazeau et al.[11] distinguished from the original formulation by specifying that the concentric growth of scales refers to their odontode generations.

0 absent

1 present

17. [B:17] **Buried odontode generations (modified).**

We split character 17 of Brazeau et al.[11] in order to code separately for overgrowth of odontode generations (character 17) and odontode resorption (character 289).

0 present

1 absent

18. [B:18] **Trunk scales with peg-and-socket articulation.**

0 absent

1 present

19. [B:19] **Scale peg.**

0 broad

1 narrow

20. [B:20] **Anterodorsal process on scale.**

0 absent

1 present

21. [B:21] **Trunk scale profile.**

0 distinct crown and base demarcated by a constriction ("neck")

1 flattened

22. [B:22] **Profile of scales with constriction between crown and base.**

0 neck similar in width to crown

1 neck greatly constricted, resulting in anvil-like shape

23. [B:23] **Trunk scales with bulging base.**

0 absent

1 present

24. [B:24] **Trunk scales with flattened base.**

0 present

1 absent

25. [B:25] **Basal pore in scales.**

0 absent

1 present

26. [B:26] **Flank scale alignment.**

0 vertical rows oblique rows or hexagonal

1 rhombic packing

2 disorganised

27. [B:27] **Scute-like ridge scales (basal fulcra).**

0 absent

1 present

28. [K:324] **Sensory line canal.**

0 passes between or beneath scales

1 passes over scales and/or is partially enclosed or surrounded by scales

2 perforates and passes through scales

29. [B:29] **Dermal ornamentation.**

0 smooth

1 parallel, vermiform ridges

2 concentric ridges

3 tuberculate

30. [B:30] **Sensory line network.**

0 preserved as open grooves (sulci) in dermal bones

1 sensory lines pass through canals in dermal bones (open as pores)

31. [B:31] **Sensory canals/grooves.**

0 contained within the thickness of dermal bones

1 contained in prominent ridges on visceral surface of bone

32. [B:32] **Jugal portion of infraorbital canal joins supramaxillary canal.**

0 present

1 absent

33. [B:33] **Dermal skull roof (modified).**

State 2 was added from character 25 of Coates el al.[12]

0 includes large dermal plates

1 consists of undifferentiated plates, tesserae or scales

2 naked or largely scale free

34. [B:34] **Anterior pit line of dermal skull roof.**

0 absent

1 present

35. [B:35] **Tessera morphology.**

0 large interlocking polygonal plates

1 microsquamose, not larger than trunk squamation

36. [B:36] **Cranial spines.**

0 absent

1 present

37. [B:37] **Cranial spines.**

0 monocuspid

1 multicupsid

38. [B:38] **Extent of dermatocranial cover.**

0 complete

1 incomplete (limited to skull roof)

39. [B:39] **Openings for endolymphatic ducts in dermal skull roof.**

0 present

1 absent

40. [B:40] **Endolymphatic ducts with oblique course through dermal skull bones.**

0 absent

1 present

41. [B:41] **Endolymphatic duct relationship to median skull roof bone (i.e. nuchal plate).**

0 within median bone

1 on bones flanking the median bone (e.g. paranuchals)

42. [B:42] **Pineal opening perforation in dermal skull roof.**

0 present

1 absent

43. [B:43] **Dermal plate associated with pineal eminence or foramen.**

0 contributes to orbital margin (plate(s) excluded from orbital margin by skull roofing bones.)

1 plate bordered laterally by skull roofing bones

44. [B:44] **Broad supraorbital vaults.**

0 absent

1 present

45. [B:45] **Median commissure between supraorbital sensory lines.**

0 absent

1 present

46. [B:46] **Dermal cranial joint at level of sphenoid-otic junction.**

0 absent

1 present

47. [B:47] **Otic canal extends through postparietals.**

0 absent

1 present

48. [B:48] **Number of bones of skull roof lateral to postparietals.**

0 two

1 one

2 more than two

49. [B:49] **Suture between paired skull roofing bones (centrals of placoderms postparietals of osteichthyans).**

0 straight

1 sinusoidal

50. [B:50] **Medial processes of paranuchal wrapping posterolateral corners of nuchal plate.**

0 absent

1 present

51. [B:51] **Paired pits on ventral surface of nuchal plate.**

0 absent

1 present

52. [B:52] **Sclerotic ring.**

0 absent

1 present

53. [B:53] **Consolidated cheek plates.**

0 absent

1 present

54. [B:54] **Cheek plate.**

0 undivided

1 divided (i.e., squamosal and preopercular)

55. [B:55] **Subsquamosals in taxa with divided cheek.**

0 absent

1 present

56. [B:56] **Preopercular shape.**

0 rhombic

1 bar-shaped

57. [B:57] **Vertical canal associated with preopercular/suborbital canal.**

0 absent

1 present

58. [B:58] **Enlarged postorbital tessera separate from orbital series.**

0 absent

1 present

59. [B:59] **Extent of maxilla along cheek.**

0 to posterior margin of cheek

1 cheek bones exclude maxilla from posterior margin of cheek

60. [B:60] **Dermal neck joint.**

0 overlap

1 ginglymoid (‘arthrodire’-type)

2 reverse ginglymoid (‘antiarch’-type)

3 longitudinal

61. [B:61] **Sensory line scales/plates on head.**

0 unspecialized

1 apposed growth

2 paralleling canal

3 semicylindrical C-shaped ring scales

62. [B:62] **Bony hyoidean gill-cover series (branchiostegals).**

0 absent

1 present

63. [B:63] **Branchiostegal plate series along ventral margin of lower jaw.**

0 absent

1 present

64. [B:64] **Branchiostegal ossifications.**

0 plate-like

1 narrow and ribbon-like

2 filamentous

65. [B:65] **Branchiostegal ossifications.**

0 ornamented

1 unornamented

66. [B:66] **Imbricated branchiostegal ossifications.**

0 absent

1 present

67. [B:67] **Median gular.**

0 absent

1 present

68. [B:68] **Lateral gular.**

0 absent

1 present

69. [B:69] **Opercular (submarginal) ossification.**

0 absent

1 present

70. [B:70] **Shape of opercular (submarginal) ossification.**

0 broad plate that tapers towards its proximal end

1 narrow, rod-shaped

71. [B:71] **Size of lateral gular plates.**

0 extending most of length of the lower jaw

1 restricted to the anterior third of the jaw (no longer than the width of three or four branchiostegals)

72. [B:72] **Gill arches.**

0 largely restricted to region under braincase

1 extend far posterior to braincase

73. [B:73] **Basihyal.**

0 absent

1 present

74. [B:74] **Interhyal.**

0 absent

1 present

75. [B:75] **Hypohyal.**

0 absent

1 present

76. [B:76] **Endoskeletal urohyal.**

0 absent

1 present

77. [B:77] **Oral dermal tubercles borne on jaw cartilages or at margins of the mouth.**

0 absent

1 present

78. [B:79] **Enamel(oid) on teeth.**

0 absent

1 present

79. [B:80] **Cap of enameloid restricted to upper part of teeth (acrodin).**

0 absent

1 present

80. [B:81] **Tooth whorls.**

0 absent

1 present

81. [C:83] **Tooth families/whorls**

0 restricted to symphysial region

1 distributed along jaw margin

82. [B:84] **Distribution of tooth whorls.**

0 lower jaws only
1 upper and lower jaws
2 upper jaws only

83. [K:354] **Parasymphyseal plate**
0 detachable tooth whorl
1 long with posterior corner, sutured to coronoid, denticulated or with tooth row
2 absent

84. [C:80] **Bases of tooth families/whorls**
0 single, continuous plate
1 some or all consist of separate tooth units

85. [B:85] **Teeth ankylosed to dermal bones.**
0 absent
1 present

86. [B:86] **Plicidentine.**
0 absent
1 present

87. [B:87] **Dermal jaw plates on biting surface of jaw cartilages.**
0 absent
1 present

88. [G:88] **Maxillary and dentary marginal bones of mouth.**
0 absent
1 present

89. [B:89] **Premaxilla.**

0 extends under orbit

1 restricted anterior to orbit

90. [B:90] **Maxilla shape.**

0 splint-shaped

1 cleaver-shaped

91. [B:91] **Pair of tooth plates (anterior supragnathals or vomers) on ethmoidal plate.**

0 absent

1 present

92. [K:353] **Strong ascending flexion of symphysial region of mandible.**

0 absent

1 present

93. [B:93] **Extent of infradentaries.**

0 along much of ventral margin of dentary

1 restricted to posterior half of dentary

94. [B:94] **Coronoid fangs.**

0 absent

1 present

95. [B:95] **Position of upper mandibular arch cartilage (and associated cheek plate where present).**

0 entirely suborbital

1 with a postorbital extension

96. [B:96] **Position of mandibular arch articulations.**

0 terminal

1 subterminal

97. [B:97] **Autopalatine and quadrate.**

0 comineralized

1 separate mineralizations

98. [B:98] **Large otic process of the palatoquadrate.**

0 absent

1 present

99. [B:99] **Insertion area for jaw adductor muscles on palatoquadrate.**

0 ventral or medial

1 lateral

100. [B:100] **Palatoquadrate fused with neurocranium.**

0 absent

1 present

101. [B:101] **Oblique ridge or groove along medial face of palatoquadrate.**

0 absent

1 present

102. [B:102] **Fenestration of palatoquadrate at basipterygoid articulation.**

0 absent

1 present

103. [B:103] **Perforate or fenestrate anterodorsal (metapterygoid) portion of palatoquadrate.**

0 absent

1 present

104. [B:104] **Pronounced dorsal process on Meckelian bone or cartilage.**

0 absent

1 present

105. [B:105] **Number of coronoids.**

0 four or more

1 three or fewer

106. [B:106] **Preglenoid process.**

0 absent

1 present

107. [B:107] **Jaw articulation located on rearmost extremity of mandible.**

0 absent

1 present

108. [B:108] **Precerebral fontanelle.**

0 absent

1 present

109. [B:109] **Median dermal bone of palate (parasphenoid).**

0 absent

1 present

110. [B:110] **Parasphenoid.**

0 lozenge-shaped

1 splint-shaped

2 diamond-shaped

111. [B:111] **Multifid anterior margin of parasphenoid denticle plate.**

0 absent

1 present

112. [B:112] **Enlarged ascending processes of parasphenoid.**

0 absent

1 present

113. [B:113] **Buccohypophysial canal in parasphenoid.**

0 single

1 paired

114. [B:114] **Nasal opening(s).**

0 dorsal, placed between orbits

1 ventral and anterior to orbit

115. [B:115] **External opening of posterior nostril and orbit.**

0 separated by dermal bone(s)

1 confluent

116. [B:116] **Olfactory tracts.**

0 short, with olfactory capsules situated close to telencephalon cavity

1 elongate and tubular (much longer than wide)

117. [B:117] **Prominent pre-orbital rostral expansion of the neurocranium.**

0 present, formed of subethmoidal platform (‘upper lip’)

1 absent

2 present, formed of rhinocapsular block

118. [B:118] **Pronounced sub-ethmoidal keel.**

0 absent

1 present

119. [B:119] **Internasal vacuities.**

0 absent

1 present

120. [B:120] **Discrete division of the ethmoid and more posterior braincase at the level of the optic tract canal.**

0 absent

1 present

121. [B:121] **Position of myodome for superior oblique eye muscles.**

0 posterior and dorsal to foramen for nerve II

1 anterior and dorsal to foramen

122. [B:122] **Endoskeletal intracranial joint.**

0 absent

1 present

123. [B:123] **Spiracular groove on basicranial surface**

0 absent

1 present

124. [B:124] **Transverse otic process.**

0 present

1 absent

125. [B:125] **Jugular canal.**

0 long (invested in otic region along length of skeletal labyrinth)

1 short (restricted to short portion of region of skeletal labyrinth, or anterior to it)

2 absent (jugular vein uninvested in otic region)

126. [B:126] **Spiracular groove on lateral commissure.**

0 absent

1 present

127. [B:127] **Subpituitary fenestra.**

0 absent

1 present

128. [B:128] **Supraorbital shelf broad with convex lateral margin.**

0 absent

1 present

129. [B:129] **Orbit dorsal or facing dorsolaterally, surrounded laterally by endocranium.**

0 present

1 absent

130. [B:130] **Eyestalk attachment area.**

0 absent

1 present

131. [B:131] **Postorbital process.**

0 absent

1 present

132. [B:132] **Canal for jugular in postorbital process.**

0 absent

1 present

133. [B:133] **Series of perforations for innervation of supraorbital sensory canal in supraorbital shelf.**

0 absent

1 present

134. [B:134] **Extended prehypophysial portion of sphenoid.**

0 absent

1 present

135. [B:135] **Narrow interorbital septum, with outer walls in contact along midline forming a single sheet.**

0 absent

1 present

136. [B:136] **The main trunk of facial nerve (N. VII).**

0 elongate and passes anterolaterally through orbital floor

1 stout, divides within otic capsule at the level of the transverse otic wall

137. [B:137] **Course of hyoid ramus of facial nerve (N. VII) relative to jugular canal.**

0 traverses jugular canal, with separate exit in otic region

1 intersects jugular canal, with exit through posterior jugular foramen

138. [B:138] **Glossopharyngeal nerve (N. IX) exit.**

0 foramen situated posteroventral to otic capsule and anterior to metotic fissure

1 through metotic fissure

139. [B:139] **Relationship of cranial endocavity to basisphenoid.**

0 endocavity occupies full depth of sphenoid

1 enodcavity dorsally restricted

140. [B:140] **Subcranial ridges.**

0 absent

1 present

141. [B:141] **Ascending basisphenoid pillar pierced by common internal carotid.**

0 absent

1 present

142. [B:142] **Canal for lateral dorsal aorta within basicranial cartilage.**

0 absent

1 present

143. [B:143] **Entrance of internal carotids.**

0 through separate openings flanking the hypophyseal opening or recess

1 through a common opening at the central midline of the basicranium

144. [B:144] **Canal for efferent pseudobranchial artery within basicranial cartilage.**

0 absent

1 present

145. [B:145] **Position of basal/basipterygoid articulation.**

0 same anteroposterior level as hypophysial opening

1 anterior to hypophysial opening

2 posterior to hypophysial opening

146. [B:146] **Articulation between neurocanium and palatoquadrate posterodorsal to orbit (suprapterygoid articulation).**

0 absent

1 present

147. [B:147] **Labyrinth cavity.**

0 separated from the main neurocranial cavity by a cartilaginous or ossified capsular wall

1 skeletal capsular wall absent

148. [B:148] **Basipterygoid process (basal articulation) with vertically oriented component.**

0 absent

1 present

149. [B:149] **Pituitary vein canal.**

0 dorsal to level of basipterygoid process

1 flanked posteriorly by basipterygoid process

150. [B:150] **External (horizontal) semicircular canal.**

0 absent

1 present

151. [B:151] **Sinus superior.**

0 absent or indistinguishable from union of anterior and posterior canals with saccular chamber

1 present

152. [B:152] **External (horizontal) semicircular canal.**

0 joins the vestibular region dorsal to posterior ampulla

1 joins level with posterior ampulla

153. [B:153] **Horizontal semicircular canal in dorsal view.**

0 medial to path of jugular vein

1 dorsal to jugular vein

154. [B:154] **Lateral cranial canal.**

0 absent

1 present

155. [B:155] **Posterior dorsal fontanelle.**

0 absent

1 present

156. [B:156] **Shape of posterior dorsal fontanelle.**

0 approximately as long as broad

1 much longer than wide, slot-shaped

157. [B:157] **Synotic tectum.**

0 absent

1 present

158. [B:158] **Dorsal ridge.**

0 absent

1 present

159. [B:159] **Shape of median dorsal ridge anterior to endolymphatic fossa.**

0 developed as a squared-off ridge or otherwise ungrooved

1 bears a midline groove

160. [B:160] **Endolymphatic ducts in neurocranium.**

0 posteriodorsally angled tubes

1 tubes oriented vertically through median endolymphatic fossa

161. [B:161] **Position of hyomandibula articulation on neurocranium.**

0 below or anterior to orbit, on ventrolateral angle of braincase

1 on otic capsule, posterior to orbit

162. [B:162] **Position of hyomandibula articulation relative to structure of skeletal labyrinth.**

0 anterior or lateral to skeletal labyrinth

1 at level of posterior semicircular canal

163. [B:163] **Hyoid arch articulation on braincase.**

0 single

1 double

164. [B:164] **Branchial ridges.**

0 present

1 reduced to vagal process

2 absent (articulation made with bare cranial wall)

165. [B:165] **Craniospinal process.**

0 absent

1 present

166. [B:166] **Ventral cranial fissure.**

0 absent

1 present

167. [B:167] **Basicranial fenestra.**

0 absent

1 present

168. [B:168] **Metotic (otic-occipital) fissure.**

0 absent

1 present

169. [B:169] **Vestibular fontanelle.**

0 absent

1 present

170. [B:170] **Occipital arch wedged in between otic capsules.**

0 absent

1 present

171. [B:171] **Spino-occipital nerve foramina.**

0 two or more, aligned horizontally

1 one or two, dorsoventrally offset

172. [B:172] **Ventral notch between parachordals.**

0 present or entirely unfused

1 absent

173. [B:173] **Parachordal shape.**

0 forming a broad, flat surface as wide as the otic capsules

1 mediolaterally constricted relative to the otic capsules

174. [B:174] **Stalk-shaped parachordal/occipital region.**

0 absent

1 present

175. [B:175] **Paired occipital facets.**

0 absent

1 present

176. [B:176] **Size of aperture to notochordal canal.**

0 much smaller than foramen magnum

1 as large, or larger, than foramen magnum

177. [B:177] **Canal for median dorsal aorta within basicranium.**

0 absent

1 present

178. [B:178] **Hypotic lamina (and dorsally directed glossopharyngeal canal).**

0 absent

1 present

179. [B:179] **Macromeric dermal shoulder girdle.**

0 present

1 absent

180. [B:180] **Dermal shoulder girdle composition.**

0 ventral and dorsal (scapular) components

1 ventral components only

181. [B:181] **Shape of dorsal blade of dermal shoulder girdle (either cleithrum or anterolateral plate).**

0 spatulate

1 pointed

182. [B:182] **Dermal shoulder girdle forming a complete ring around the trunk.**

0 present

1 absent

183. [B:183] **Pectoral fenestra completely encircled by dermal shoulder armour.**

0 present

1 absent

184. [B:184] **Median dorsal plate.**

0 absent

1 present

185. [B:185] **Posterior dorsolateral (PDL) plate or equivalent.**

0 absent

1 present

186. [B:186] **Pronounced internal median keel on dorsal shoulder girdle (i.e., crista of median dorsal plate).**

0 absent

1 present

187. [B:187] **Crista internalis of dermal shoulder girdle.**

0 absent

1 present

188. [B:188] **Scapular infundibulum.**

0 absent

1 present

189. [B:189] **Scapular process of shoulder endoskeleton.**

0 absent

1 present

190. [B:190] **Ventral margin of separate scapular ossification.**

0 horizontal

1 deeply angled

191. [B:191] **Cross sectional shape of scapular process.**

0 flattened or strongly ovate

1 subcircular

192. [B:192] **Flange on trailing edge of scapulocoracoid.**

0 absent

1 present

193. [B:193] **Scapular process with posterodorsal angle.**

0 absent

1 present

194. [B:194] **Endoskeletal postbranchial lamina on scapular process.**

0 present

1 absent

195. [B:195] **Mineralisation of internal surface of scapular blade.**

0 mineralised all around

1 unmineralised on internal face forming a hemicylindrical cross-section

196. [B:196] **Coracoid process.**

0 absent

1 present

197. [B:197] **Procoracoid mineralisation.**

0 absent

1 present

198. [B:198] **Fin base articulation on scapulocoracoid.**

0 deeper than wide (stenobasal)

1 wider than deep (eurybasal)

199. [B:199] **Pectoral fin articulation.**

0 monobasal

1 polybasal

200. [B:200] **Number of basals in polybasal pectoral fins.**

0 three or more

1 two

201. [B:201] **Branching radials in paired fins.**

0 absent

1 present

202. [B:202] **Number of mesomeres in metapterygial axis.**

0 five or fewer

1 seven or more

203. [B:203] **Biserial pectoral fin endoskeleton.**

0 absent

1 present

204. [B:204] **Perforate propterygium.**

0 absent

1 present

205. [B:205] **Filamentous extension of pectoral fin from axillary region.**

0 absent

1 present

206. [B:206] **Pelvic fins.**

0 absent

1 present

207. [B:207] **Pelvic claspers.**

0 absent

1 present

208. [B:208] **Dermal pelvic clasper ossifications.**

0 absent

1 present

209. [B:209] **Pectoral fins covered in macromeric dermal armour.**

0 absent

1 present

210. [B:210] **Pectoral fin base has large, hemispherical dermal component.**

0 absent

1 present

211. [B:211] **Dorsal fin spines.**

0 absent

1 present

212. [B:212] **Anal fin spine.**

0 absent

1 present

213. [B:213] **Paired fin spines.**

0 absent

1 present

214. [B:214] **Median fin spine insertion.**

0 shallow, not greatly deeper than dermal bones/scales

1 deep

215. [B:215] **Prepelvic fin spines (modified).**

We follow Burrow et al.[16] and Hanke & Wilson[17] in labelling the fin spine pairs developed between the pectoral and pelvic fin spines as 'prepelvic' instead of the 'intermediate' used by Brazeau et al.[11]

0 absent

1 present

216. [B:216] **Fin spine cross-section.**

0 Round or horseshoe shaped

1 Flat-sided, with rectangular profile

217. [B:217] **Prepelvic spines when present (modified).**

See comments on character 215.

0 one pair

1 multiple pairs

218. [B:218] **Paired prepectoral spines (modified).**

Modified to enable coding for lateral pairs of prepectoral spines.

0 absent

1 present

219. [B:219] **Fin spines with ridges.**

0 absent

1 present

220. [B:220] **Fin spines with nodes.**

0 absent

1 present

221. [B:221] **Fin spines with rows of large retrorse denticles.**

0 absent

1 present

222. [B:222] **Expanded spine rib on leading edge of spine.**

0 absent

1 present

223. [B:223] **Spine ridges**

0 converging at the distal apex of the spine

1 converging on leading edge of spine

224. [B:224] **Synarcual.**

0 absent

1 present

225. [B:225] **Series of thoracic supraneurals.**

0 absent

1 present

226. [B:226] **Number of dorsal fins, if present.**

0 one

1 two

227. [B:227] **Posterior dorsal fin shape.**

0 base approximately as broad as tall, not broader than all of other median fins

1 base much longer than the height of the fin, substantially longer than any of the other dorsal fins

228. [B:228] **Basal plate in dorsal fin.**

0 absent

1 present

229. [B:229] **Branching radial structure articulating with dorsal fin basal plate.**

0 absent

1 present

230. [B:230] **Anal fin.**

0 absent

1 present

231. [B:231] **Basal plate in anal fin.**

0 absent

1 present

232. [B:232] **Caudal radials.**

0 extend beyond level of body wall and deep into hypochordal lobe

1 radials restricted to axial lobe

233. [B:233] **Supraneurals in axial lobe of caudal fin.**

0 absent

1 present

234. [B:234] **Epichordal lepidotrichia in caudal fin.**

0 absent

1 present

235. [B:235] **Enamel and pore canals.**

0 enamel absent from inner surface of pores

1 enamel lines portions of pore canal

236. [B:236] **Canal-bearing bone of skull roof extends far past posterior margin of parietals.**

0 no

1 yes

237. [B:237] **Pineal eminence (in taxa lacking pineal foramen).**

0 absent

1 present

238. [B:238] **Position of anterior pitline.**

0 on postparietal

1 on parietal

239. [B:239] **Opening in dermal skull roof for spiracular bounded by bones carrying otic canal.**

0 absent

1 present

240. [B:240] **Median skull roof bone between postparietals.**

0 absent

1 present

241. [B:241] **Westoll lines.**

0 absent

1 present

242. [B:242] **Preoperculosubmandibular.**

0 absent

1 present

243. [B:243] **Hyomandibula.**

0 imperforate

1 perforate

244. [B:244] **Urohyal shape.**

0 absent

1 vertical plate

245. [B:246] **Length of dentary.**

0 constitutes a majority of jaw length

1 half the length of jaw or less

246. [B:247] **Labial pit.**

0 absent

1 present

247. [B:248] **Prearticular symphysis.**

0 absent

1 present

248. [B:249] **Mandibular sensory canal.**

0 extends through infradentaries

1 extends through infradentaries and dentary

249. [B:250] **Extensive flange composed of prearticular and Meckelian bone that extends beyond ventral edge of outer dermal series.**

0 absent

1 present

250. [B:251] **Posterior coronoid.**

0 similar to anterior coronoids

1 forms expanded coronoid process

251. [B:252] **Retroarticular process.**

0 absent

1 present

252. [B:253] **Inturned medial process of premaxilla.**

0 absent

1 present

253. [B:254] **Anteriorly directed adductor fossae between neurocranium and skull roof.**

0 absent

1 present

254. [B:255] **Vomerine fangs.**

0 absent

1 present

255. [B:256] **Number of dermopalatines.**

0 multiple

1 one

256. [B:257] **Entopterygoids.**

0 separated

1 contact along midline

257. [B:258] **Rostral tubuli.**

0 absent

1 present

258. [B:259] **Position of anterior nostril.**

0 facial

1 at oral margin

259. [B:260] **Posterior nostril.**

0 facial

1 at margin of oral cavity

2 palatal

260. [B:261] **Three large pores (in addition to nostrils) associated with each side of ethmoid.**

0 absent

1 present

261. [B:262] **Ventral face of nasal capsule in taxa with mineralized ethmoid.**

0 complete

1 fenestra ventrolateralis

2 entire floor unmineralized

262. [B:263] **Size of profundus canal in postnasal wall.**

0 small

1 large

263. [B:264] **Paired pineal and parapineal tracts.**

0 absent

1 present

264. [B:265] **Posterior of parasphenoid.**

0 restricted to ethmosphenoid region

1 extends to otic region

265. [B:266] **Endoskeletal spiracular canal.**

0 open

1 spiracular bar

2 complete enclosure in canal

266. [B:267] **Barbed lepidotrichial segments.**

0 absent

1 present

267. [B:268] **Relative position of jugular groove/canal and hyomandibular articulation.**

0 hyomandibula dorsal

1 hmd straddles

2 hmd ventral

268. [B:269] **Optic lobes.**

0 narrower than cerebellum

1 same width or wider than cerebellum

269. [B:270] **Hypophyseal chamber.**

0 projects posteroventrally

1 projects ventrally or anteroventrally

270. [B:271] **Crus commune of anterior and posterior semicircular canals.**

0 dorsal to braincase endocavity roof

1 ventral to braincase endocavity roof

271. [B:272] **Horizontal semicircular canal.**

0 obliquely oriented

1 horizontally oriented

272. [B:273] **Supraotic cavity.**

0 absent

1 present

273. [B:274] **Pelvic girdle with substantial dermal component.**

0 present

1 absent

274. [B:275] **Pelvic fin spines.**

0 absent

1 present

275. [B:276] **Pelvic fin.**

0 monobasal

1 polybasal

276. [B:277] **Postparietals/centrals.**

0 absent

1 present

277. [B:278] **Condition of postparietals/centrals.**

0 do not meet in midline

1 meet in midline

2 single midline bone

278. [B:279] **Parietals.**

0 absent

1 present

279. [B:280] **Condition of parietals.**

0 do not meet in midline

1 meet in midline

280. [B:281] **Endoskeletal lamina (postnasal wall) separating posterior nostril and orbit.**

0 absent

1 present

281. [B:282] **Pituitary vein canal.**

0 discontinuous, enters the cranial cavity

1 discontinuous, enters hypophysial recess

2 continuous transverse vein

282. [B:283] **Sutures between dermal bones.**

0 absent

1 present

283. [B:284] **Interolateral/clavicular margin.**

0 angled anterolaterally

1 mediolaterally straight

284. Scale odontodes added in a linear sequence within rows (linear odontocomplexes) (new character).

0 absent

1 present

285. Number of linear odontocomplexes in scale crowns (new character).

0 one

1 more than one

286. [D:262] **Anteriormost prepelvic fin spine (admedian fin spine) associated with the shoulder girdle (modified).**

We agree with Dearden et al.[13] in recognising the shoulder girdle spines positioned medially of the pectoral fin spines in a number of stem chondrichthyans (e.g. climatiids[18,19], diplacanthids[20] and gyracanthids[21]) as the first prepelvic fin spine pair. Here these are labelled admedian after Burrow et al.[18,20,22], who contrary to this and other studies[13,23] consider them separate from the prepelvic series.

0 absent

1 present

287. [K:482] **Median ventral prepectoral spine.**

0 absent

1 present

288. [K:447] **Median ventral trunk plates.**

0 absent

1 present

289. [B:17] **Odontode resorption in the extra-oral dermal skeleton (modified).**

See comments on character 17.

0 absent

1 present

290. Pinnal plates of the dermal shoulder girdle (new character).

Pinnal plate development differs from that of the dermal plates of jawed stem gnathostomes ('placoderms')[24,25] and osteichthyans[26-28]. The latter form as a single unit through areal growth unlike the pinnals where independent dermal scales are integrated into discrete elements fused together by a basal plate[18,20,29] (see also this study). On this basis, and in accordance with previous research[30], we code for presence/absence of pinnal plates independently of the pectoral ventral plate pairs of 'placoderms' (ventrolateral plates) and osteichthyans (clavicles).

0 absent

1 present

291. Dermal bone structure of scales and non-dental plates (new character). The stem chondrichthyans *Climatius*, *Diplacanthus* and *Ptomacanthus* possess extra-oral dermal elements (e.g. shoulder girdle plates, branchiostegal plates and scales) with two distinct bone architectures (compact and spongy)[13,18,20]. They are therefore considered polymorphic for this character instead of possessing state (0) where the bone tissue has a tiered structure produced by the formation of compact and vascular bone.

0 compact and vascular

1 compact

2 vascular

292. Size of primary teeth within whorls (new character)

0 remains consistent

1 increases gradually

293. Accessory teeth in tooth whorls (new character). These have been documented[31,32] to develop laterally and/or labially of the primary whorl teeth and are distinguished from the latter by their noticeably smaller size and different organisation/patterning.

0 absent

1 present

294. Mandibular teeth (new character)

0 monocuspid

1 multicuspid

Table S1. Tip (taxon) ages of the 50 percent majority-rule tree shown in Extended Data Fig. 4.

Taxon	Age in million years	Reference
Acanthodes	298	King et al.[15]
Achoania	412	King et al.[15]
Akmonistion	327	King et al.[15]
Austroptyctodus	327	King et al.[15]
Bothriolepis	383	King et al.[15]
Brachyacanthus	415	King et al.[15]
Brindabellaspis	401	King et al.[15]
Brochoadmones	415	King et al.[15]
Buchanosteus	408	King et al.[15]
Campbellodus	383	King et al.[15]
Cassidiceps	415	King et al.[15]
Cheiracanthus	388	King et al.[15]
Cheirolepis	388	King et al.[15]
Chondrenchelys	338	King et al.[15]
Cladodoides	375	King et al.[15]
Cladoselache	360	King et al.[15]
Climatius	415	King et al.[15]
Cobelodus	325	King et al.[15]
Coccosteus	388	King et al.[15]
Compagopiscis	383	King et al.[15]

Cowralepis	383	King et al.[15]
Culmacanthus	385	King et al.[15]
Debeerius	320	King et al.[15]
Diabolepis	412	King et al.[15]
Dialipina	401	King et al.[15]
Dicksonosteus	411	King et al.[15]
Diplacanthus	388	King et al.[15]
Diplocercides	383	Long and Trinajstic[33]
Dipterus	388	Gross[34]
Doliodus	395	King et al.[15]
Entelognathus	424	King et al.[15]
Eurycaraspis	385	King et al.[15]
Eusthenopteron	380	King et al.[15]
Euthacanthus	415	King et al.[15]
Galeaspida	436	King et al.[15]
Gavinia	385	Long[35]
Gemuendina	408	King et al.[15]
Gladbachus	388	Coates et al.[12]
Gladiobranchus	415	King et al.[15]
Glyptolepis	388	King et al.[15]
Gogonasus	383	King et al.[15]
Guiyu	424	King et al.[15]
Gyracanthides	388	Warren et al.[21]
Halimacanthodes	383	Burrow et al.[36]
Hamiltonichthys	302	King et al.[15]
Helodus	311	King et al.[15]
Homalacanthus	380	King et al.[15]
Howqualepis	385	King et al.[15]
Incisoscutum	383	King et al.[15]
Iniopera	307	Pradel et al.[37]
Ischnacanthus	415	King et al.[15]

Jagorina	375	King et al.[15]
Janusiscus	415	King et al.[15]
Kansasiella	303	King et al.[15]
Kathemacanthus	415	King et al.[15]
Kentuckia	347	King et al.[15]
Kosoraspis	419	Vaškaninová et al.[38]
Kujdanowiaspis	411	King et al.[15]
Latviacanthus	404	King et al.[15]
Lawrenciella	303	Poplin 1984
'Ligulalepis'	401	King et al.[15]
Lophosteus	423	Schultze and Märss[39]
Lunaspis	408	King et al.[15]
Lupopsyrus	415	King et al.[15]
Macropetalichthys	390	King et al.[15]
Meemannia	412	King et al.[15]
Mesacanthus	415	King et al.[15]
Miguashaia	380	King et al.[15]
Mimipiscis	383	King et al.[15]
Minjinia	411	Brazeau et al.[11]
Moythomasia	383	King et al.[15]
Nerepisacanthus	423	King et al.[15]
Obtusacanthus	415	King et al.[15]
Onychodus	383	King et al.[15]
Onychoselache	336	King et al.[15]
Orthacanthus	290	King et al.[15]
Osteostraci	427	King et al.[15]
Parayunnanolepis	412	King et al.[15]
Parexus	415	King et al.[15]
Poracanthodes	417	King et al.[15]
Porolepis	411	King et al.[15]
Powichthys	411	King et al.[15]

Promesacanthus	415	King et al.[15]
Psarolepis	416	King et al.[15]
Pterichthyodes	389	King et al.[15]
Ptomacanthus	415	King et al.[15]
Ptyctolepis	411	Lu et al.[40]
Pucapampella	388	King et al.[15]
Qianodus	439	this study
Qilinyu	424	Zhu et al.[41]
Qingmenodus	411	Lu and Zhu[42]
Ramirosuarezia	392	King et al.[15]
Raynerius	373	Giles et al.[14]
Rhadinacanthus	388	Burrow et al.[20]
Rhamphodopsis	388	King et al.[15]
Romundina	415	King et al.[15]
Sparalepis	424	King et al.[15]
Styloichthys	412	King et al.[15]
Tamiobatis	360	King et al.[15]
Tetanopsyrus	415	King et al.[15]
Tristychius	336	King et al.[15]
Uranolophus	411	Denison[43]
Vernicomacanthus	415	King et al.[15]
Youngolepis	412	King et al.[15]
Yunnanolepis	415	King et al.[15]

Descriptions of Supplementary Files

Supplementary Data 1. Volume rendering of the holotype of *Qianodus* (IVPP V26641) based on synchrotron X-ray tomography data acquired at the Taiwan Light Source (TLS), National Synchrotron Radiation Research Center (NSRRC), Taiwan.

Colour coded features: orange, progenitor tooth row; green, trailing tooth row; yellow, accessory teeth; grey, whorl base. Rendering generated in Mimics 19.0.

Supplementary Data 2. Volume rendering of synchrotron X-ray tomography data depicting radiotransparent spaces inside the holotype of *Qianodus* (IVPP V26641) analysed at the Taiwan Light Source (TLS), National Synchrotron Radiation Research Center (NSRRC), Taiwan. Colour coded features: purple, primary teeth; yellow, accessory teeth; white, spongiose tissue of the whorl base; pink, compact tissue of the whorl base. Rendering generated in Mimics 19.0.

Supplementary Data 3. Tomographic slices from an X-ray tomography analysis of the *Qianodus* holotype specimen (IVPP V26641) at the Taiwan Light Source (TLS), National Synchrotron Radiation Research Center (NSRRC), Taiwan. Dataset generated in Mimics 19.0.

Supplementary Data 4. Tomographic slices from an X-ray tomography analysis of a *Qianodus* specimen IVPP V26645 at the Taiwan Light Source (TLS), National Synchrotron Radiation Research Center (NSRRC), Taiwan. Dataset generated in Mimics 19.0.

Supplementary Data 5. Tomographic slices from an X-ray tomography analysis of a *Qianodus* specimen IVPP V26647 at the Institute of Vertebrate Paleontology and

Paleoanthropology, Chinese Academy of Sciences. Dataset generated in Mimics 19.0.

Supplementary Data 6. Parsimony analysis files. Character-taxon matrix in TNT (.tnt) and nexus (.nex) file formats**.** Most parsimonious trees (.tre) produced by the parsimony analysis. 50 percent majority-rule consensus tree (.tre) and strict consensus tree (.tre) for the set of most parsimonious trees. Likelihood and parsimony reconstructions of character states at internal nodes of the 50 percent majority-rule consensus tree in excel (.xlxs) file format. TNT log file in rich text format (.rtf) of the parsimony analysis and the bootstrap resampling analysis. R script in rich text format (.rtf) used in the calculation of the time-scaled 50 percent majority-rule consensus tree.

References

1 Aldridge, R. J. & Wang, C.-Y. in *Telychian Rocks of the British Isles and China (Silurian, Llandovery Series: An Experiment to Test Precision in Stratigraphy National Museum of Wales Geological Series* (eds Holland, C. H. & Bassett, M. G.) 83-94 (Nat. Mus. Wales, 2002).

2 Rong, J., Johnson, M. E. & Yang, X. Early Silurian (Llandovery) sealevel changes in the Upper Yangtze region of central and southwestern China. *Acta Palaeont. Sin.* **23**, 672-694 (1984).

3 Rong, J., Wang, Y. & Zhang, X. Tracking shallow marine red beds through geological time as exemplified by the lower Telychian (Silurian) in the Upper Yangtze Region, South China. *Sci. China Earth Sci.* **55**, 699-713 (2012).

4 Mu, E. *Correlation of the Silurian Rocks of China*. Vol. 202 (Geological Society of America, 1986).

5 Wang, C.-Y. Restudy on the ages of Silurian red beds in South China. *J. Stratigr.* **35**, 440-447 (2011).

6 Wang, C.-Y. *Silurian Conodonts in China* (Univ. Sci. Tech. China Press, 2013).

7 Wang, C.-Y., Chen, L., Wang, Y. & Tang, P. Affirmation of *Pterospathodus eopennatus* Zone (Conodonta) and the age of the Silurian Shamao Formation in Zigui, Hubei as well as the correlation of the related strata. *Acta Palaeont. Sin.* **49**, 10-28 (2010).

8 Rong, J. *et al.* Silurian integrative stratigraphy and timescale of China. *Sci. China Earth Sci.* **62**, 89-111 (2018).

9 Tang, P., Xu, H. & Wang, Y. Chitinozoan-based age of the Wengxiang Group in Kaili, southeastern Guizhou, Southwest China. *J. Earth Sci.* **21**, 52 (2010).

10 Zhou, X., Zhai, Z.-Q. & Xian, S. On the Silurian conodont biostratigraphy, new genera and species in Guizhou Province. *Oil Gas Geol.* **2**, 123-140 (1981).

11 Brazeau, M. *et al.* Endochondral bone in an Early Devonian 'placoderm' from Mongolia. *Nat. Ecol. Evol.* **4**, 1477–1484 (2020).

12 Coates, M. I. *et al.* An early chondrichthyan and the evolutionary assembly of a shark body plan. *Proc. R. Soc B* **285**, 20172418 (2018).

13 Dearden, R. P., Stockey, C. & Brazeau, M. D. The pharynx of the stem-chondrichthyan *Ptomacanthus* and the early evolution of the gnathostome gill skeleton. *Nat. Commun.* **10**, 2050 (2019).

14 Giles, S., Friedman, M. & Brazeau, M. D. Osteichthyan-like cranial conditions in an Early Devonian stem gnathostome. *Nature* **520**, 82-85 (2015).

15 King, B., Qiao, T., Lee, M. S., Zhu, M. & Long, J. A. Bayesian morphological clock methods resurrect placoderm monophyly and reveal rapid early evolution in jawed vertebrates. *Syst. Biol.* **66**, 499-516 (2017).

16 Brazeau, M. D. & Friedman, M. The origin and early phylogenetic history of jawed vertebrates. *Nature* **520**, 490-497 (2015).

17 Hanke, G. & Wilson, M. in *Morphology, Phylogeny and Paleobiogeography of Fossil Fishes.* (eds Elliott, D. K., Maisey, J. G., Yu, X. & Miao, D.) 159-182 (Verlag Dr. Friedrich Pfeil, 2010).

18 Burrow, C. J., Davidson, R. G., Den Blaauwen, J. L. & Newman, M. J. Revision of *Climatius reticulatus* Agassiz, 1844 (Acanthodii, Climatiidae), from the Lower Devonian of Scotland, based on new histological and morphological data. *J. Vertebr. Paleont.* **35**, e913421 (2015).

19 Miles, R. S. Articulated acanthodian fishes from the Old Red Sandstone of England: with a review of the structure and evolution of the acanthodian shoulder-girdle. *Bull. Br. Mu. Nat. Hist. Geol.* **24**, 111-213 (1973).

20 Burrow, C., den Blaauwen, J., Newman, M. & Davidson, R. The diplacanthid fishes (Acanthodii, Diplacanthiformes, Diplacanthidae) from the Middle Devonian of Scotland. *Palaeontol. Electron.* **19**, 1-83 (2016).

21 Warren, A., Currie, B. P., Burrow, C. & Turner, S. A redescription and reinterpretation of *Gyracanthides murrayi* Woodward 1906 (Acanthodii, Gyracanthidae) from the Lower Carboniferous of the Mansfield Basin, Victoria, Australia. *J. Vertebr. Paleontol.* **20**, 225-242 (2000).

22 Burrow, C. J., Newman, M. J., Davidson, R. G. & den Blaauwen, J. L. Redescription of *Parexus recurvus*, an Early Devonian acanthodian from the Midland Valley of Scotland. *Alcheringa* **37**, 392-414 (2013).

23 Gagnier, P.-Y. & Wilson, M. V. Early Devonian acanthodians from northern Canada. *Palaeontology* **39**, 241-258 (1996).

24 Dupret, V., Sanchez, S., Goujet, D., Tafforeau, P. & Ahlberg, P. E. Bone vascularization and growth in placoderms (Vertebrata): The example of the premedian plate of *Romundina stellina* Ørvig, 1975. *C. R. Palevol* **9**, 369-375 (2010).

25 Giles, S., Rücklin, M. & Donoghue, P. C. Histology of “placoderm” dermal skeletons: Implications for the nature of the ancestral gnathostome. *J. Morph.* **274**, 627-644 (2013).

26 Andrews, M., Long, J., Ahlberg, P., Barwick, R. & Campbell, K. The structure of the sarcopterygian *Onychodus jandemarrai* n. sp. from Gogo, Western Australia: with a functional interpretation of the skeleton. *Earth. Env. Sci. Trans. R. Soc. Edinb.* **96**, 197-307 (2005).

27 Mondéjar-Fernández, J., Friedman, M. & Giles, S. Redescription of the cranial skeleton of the Early Devonian (Emsian) sarcopterygian *Durialepis edentatus* Otto (Dipnomorpha, Porolepiformes). *Pap. Palaeontol.* (2020).

28 Zhu, M., Yu, X., Wang, W., Zhao, W. & Jia, L. A primitive fish provides key characters bearing on deep osteichthyan phylogeny. *Nature* **441**, 77-80 (2006).

29 Long, J. A new diplacanthoid acanthodian from the Late Devonian of Victoria. *Mem. Assoc. Australas. Palaeontol.* **1**, 51-65 (1983).
30 Moy-Thomas, J. & Miles, R. S. Palaeozoic Fishes (Chapman and Hall, 1971).
31 Ahlberg, P. E. A new holoptychiid porolepiform fish from the Upper Frasnian of Elgin, Scotland. *Palaeontology* **35**, 813-828 (1992).
32 Qu, Q., Sanchez, S., Blom, H., Tafforeau, P. & Ahlberg, P. E. Scales and tooth whorls of ancient fishes challenge distinction between external and oral 'teeth'. *PLoS One* **8**, e71890 (2013).
33 Long, J. A. & Trinajstic, K. The Late Devonian Gogo Formation lägerstatte of Western Australia: exceptional early vertebrate preservation and diversity. *Annu. Rev. Earth Planet Sci.* **38**, 255-279 (2010).
34 Gross, W. Über die Randzähne des Mundes, die Ethmoidalregion des Schädels und die Unterkiefersymphyse von *Dipterus oervigi* n. sp. *Paläontol. Z.* **38**, 7-25 (1964).
35 Long, J. A. A new genus of fossil coelacanth (Osteichthyes: Coelacanthiformes) from the Middle Devonian of southeastern Australia. *Rec. West. Aust. Mus., Suppl* **57**, 37-53 (1999).
36 Burrow, C. J., Trinajstic, K. & Long, J. First acanthodian from the Upper Devonian (Frasnian) Gogo Formation, Western Australia. *Hist. Biol.* **24**, 349-357 (2012).
37 Pradel, A., Tafforeau, P. & Janvier, P. Study of the pectoral girdle and fins of the Late Carboniferous sibyrhynchid iniopterygians (Vertebrata, Chondrichthyes, Iniopterygia) from Kansas and Oklahoma (USA) by means of microtomography, with comments on iniopterygian relationships. *C. R. Palevol* **9**, 377-387 (2010).
38 Vaškaninová, V. *et al.* Marginal dentition and multiple dermal jawbones as the ancestral condition of jawed vertebrates. *Science* **369**, 211-216 (2020).
39 Schultze, H.-P. & Märss, T. Revisiting *Lophosteus*, a primitive osteichthyan. *Acta Univ. Latv.* **679**, 57-78 (2004).
40 Lu, J., Giles, S., Friedman, M. & Zhu, M. A new stem sarcopterygian illuminates patterns of character evolution in early bony fishes. *Nat. Commun.* **8**, 1932 (2017).
41 Zhu, M. *et al.* A Silurian maxillate placoderm illuminates jaw evolution. *Science* **354**, 334-336 (2016).
42 Lu, J. & Zhu, M. An onychodont fish (Osteichthyes, Sarcopterygii) from the Early Devonian of China, and the evolution of the Onychodontiformes. *Proc. Roy. Soc. B: Biol. Sci.* **277**, 293-299 (2010).
43 Denison, R. H. Early Devonian lungfishes from Wyoming, Utah, and Idaho. *Field Mus. Nat. Hist. Bull.* **17**, 353–413 (1968).